Chapter 16

Airplane Optimal Robust Design Combined with an Entropy-Statistics Unsupervised Learning Classification Algorithm

Chapter details

Chapter DOI:

https://doi.org/10.4322/978-65-86503-88-3.c16

Chapter suggested citation / reference style:

Mattos, Bento S., et al. (2022). “Airplane Optimal Robust Design Combined with an Entropy-Statistics Unsupervised Learning Classification Algorithm”. *In* Jorge, Ariosto B., et al. (Eds.) *Uncertainty Modeling: Fundamental Concepts and Models*, Vol. III, UnB, Brasilia, DF, Brazil, pp. 502–551. Book series in Discrete Models, Inverse Methods, & Uncertainty Modeling in Structural Integrity.

P.S.: DOI may be included at the end of citation, for completeness.

Book details

Book: Uncertainty Modeling: Fundamental Concepts and Models

Edited by: Jorge, Ariosto B., Anflor, Carla T. M., Gomes, Guilherme F., & Carneiro, Sergio H. S.

Volume III of Book Series in:

Discrete Models, Inverse Methods, & Uncertainty Modeling in Structural Integrity

Published by: UnB City: Brasilia, DF, Brazil Year: 2022

DOI: https://doi.org/10.4322/978-65-86503-88-3

Airplane Optimal Robust Design Combined with an Entropy-Statistics Unsupervised Learning Classification Algorithm

Bento S. de Mattos[1*] José A. T. G. Fregnani[1] Ariosto B. Jorge[2]

[1]Instituto Tecnológico de Aeronáutica. E-mail: bmattos@ita.br, eng.fregnani@hotmail.com
[2]Post-Graduate Program - Integrity of Engineering Materials, University of Brasilia, Brazil. E-mail: ariosto.b.jorge@gmail.com

*Corresponding author

Abstract

The present work describes an airliner design platform that has been developed over several years and its application to design airliners based on an efficiency index developed by the authors of the present work. Among other characteristics, the design tool can handle airplane geometries with detail and count on a unique and accurate neural network system to predict aerodynamic coefficients. A new feature for product classification was incorporated into the framework. It is based on entropy statistics and was calibrated for jet transport airplanes and the results of classification are analyzed in the present work. The design of a Middle of Market airplane was then carried out with the classification provided by entropy statistics set as a constraint. Middle of the Market is a term that was established to address the commercial aircraft market segment that encompasses long-haul sectors from 3500 nm to 5000 nm, and airplanes with single-class passenger capacity between 220 and 250. Until now, this segment was not extensively explored, and some airlines have been showing interest to purchase airplanes better suited to it = this category. Multi-objective optimizations were carried out to determine the best aircraft design that fits into this concept's range and capacity specifications. The unsupervised learning algorithm based on entropy statistics was applied for airplane classification into four labels, classic, niche, failure, and breakthrough designs. A higher fidelity engine model optimization task was also carried out to search for optimal classic designs. In addition, a robust optimization considering a fuel price variation on Direct Operating Cost was carried out. All results raised an important discussion about the benefits and drawbacks of a trijet configuration for transport airplanes with a capacity of over 200 passengers.

Keywords: Commercial aviation, conceptual aircraft design, artificial neural network, multi-disciplinary design, and optimization, entropy statistics

Symbols and abbreviations

AAT	Airplane Analysis Tool
ANN	Artificial neural network
AR	Aspect ratio
ATC	Air Traffic Controller
BEW	Basic Empty Weight
BPR	Engine by-pass ratio
CAD	Computer-Aided Design
CAE	Computer Aided Engineering
CFD	Computational fluid dynamics
DOC	Direct operating cost [US$/nm]
$\mathbf{D_E}$	Engine external diameter
EI	Efficiency index for airliners
$\mathbf{EI_{BJ}}$	Efficiency index for business jets
ETOPS	Extended-range Twin-engine Operations Performance Standards
FPR	Fan pressure ratio
HT	Horizontal tail
L/D	Lift-to-drag ratio
$\mathbf{L_f}$	Fuselage length [m]
MDO	Multi-disciplinary design and optimization
MMA	Middle of the market aircraft
MMO	Maximum operating Mach number
MTOW	Maximum takeoff weight [kg]
$\mathbf{n_e}$	Number of engines
NPAX	Passenger capacity in 2-class configuration (10% in business class)
OEW	Operating empty weight [kg]
OPR	Engine overall pressure ratio
PAX	Passenger or passengers
T	Overall takeoff thrust of an airplane [kN]
TBO	The time between overhaul for engines [h]
TFL	Takeoff field length
$\mathbf{T_S}$	The thrust of an engine @ takeoff [kN]
TSFC	Thrust specific fuel consumption [kg/h/kg]
TW	Thrust-to-weight ratio
VT	Vertical tail
wAR	Wing aspect ratio
wS	Wing area [m^2]
wTR	Wing taper ratio
wSw14	Wing quarter-chord sweepback angle

1. Introduction

Aviation experienced a huge sprung when jet airplanes were introduced into commercial service in the late 1950s. Since then, worldwide passenger transportation has steadily increased at an exponential pace [1] thanks to more efficient airliners and to the Deregulation Act of 1978, which provided a boost for low-cost/low-fare airlines. Indeed, aviation is steadily evolving and is currently characterized by acute competition between two giant aircraft manufacturers in the medium and high-capacity market segment. Both companies introduced airliners to fulfill passenger and cargo demands in the 150-220 passenger capacity segment, airplanes that compose the fleet of most airlines around the world, especially those labeled as low-cost/low-fare airlines. In the high-capacity segment, high-performance airplanes enabled the establishment of new long-range routes [2].

As propulsion, material, and avionics technologies evolved, as well as computational tools (such as CFD, MDO, and electronic mockups) manufacturers could develop more fuel-efficient, long-range aircraft with a larger payload. Today, airplanes like Boeing 787 and Airbus A350 are 70% more fuel-efficient, in terms of kilograms of fuel burned per passenger, than the first-generation jet transports [3].

Figure 1 shows a range capacity graph where a gap between the short- and middle-range exists for single-aisle airliners. More specifically, there is an unfulfilled region for passenger capacity between 230 and 310 seats and a range above 3700 nm. In fact, until now there are no models available on the market that could accommodate 250 passengers into a single-class cabin layout offering a range beyond 4500 nm for shot/medium-haul operations. The MMA gap could be filled with airplanes ranging from 3700 to 5000 nm, capable of transporting 220-270 passengers. Originally this market was serviced by the Boeing 757 Series, which was designed to replace the venerable Boeing 707 for cross-country routes in the United States. The production of this airplane was discontinued, and its design was outclassed by newer, more fuel-efficient aircraft.

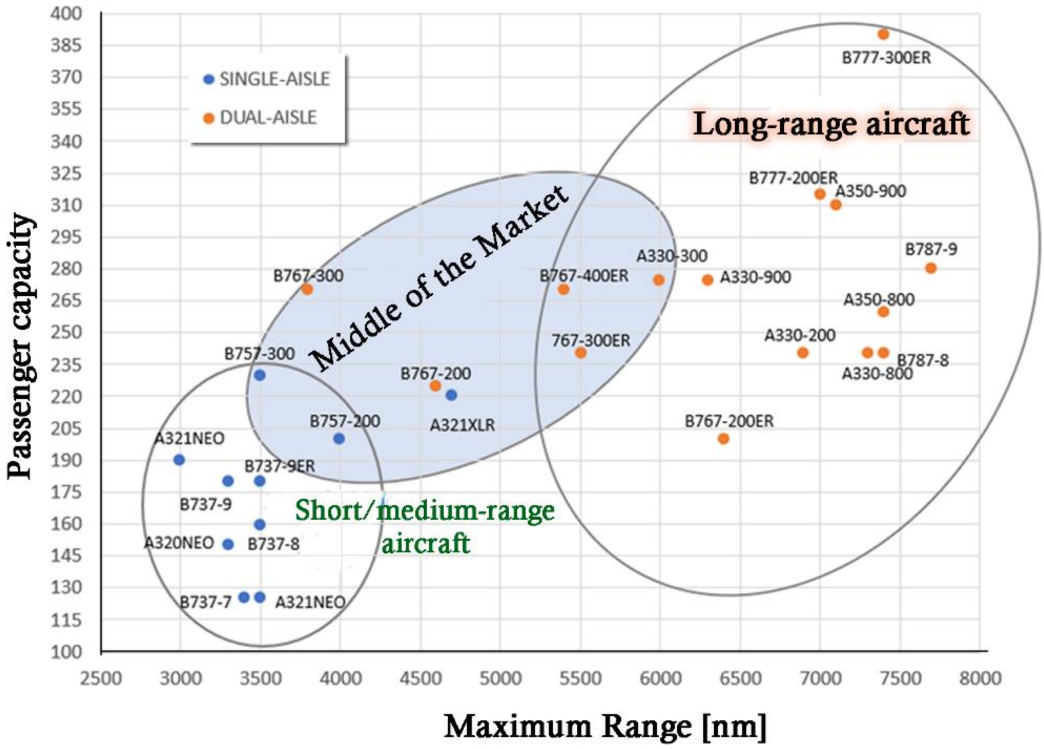

Figure 1: The middle of the market aircraft is waiting for a new airliner [4]

It is important to specify the kind of city pairs that are being considered for MMA operations. A non-stop concept for long-range direct routes was introduced by the new high-efficient wide-body designs like Boeing 787 and Airbus A350. This was due to the emergence of some markets that could be serviced by those ultra-long-range airliners. With the expansion of low-cost carriers into more distant destinations, using improved engine and airframe technologies present in current narrow-body airplanes, it could be possible to reach such markets with lower seating capacity and with narrow-body operating costs. Routes such as Honolulu-Seattle, Los Angeles-New York, New York-Manchester, London-Berlin, Dubai-Mumbai, and Beijing-Hong Kong could be served this way. These routes as well as some others would be feasible with such new, more efficient airliners, as shown in Figure 2 [5].

Figure 2: Potential routes with new generation narrow bodies [5]

Multi-disciplinary optimization tools are part of the everyday activities of aircraft manufacturers, whatever size they are. Thanks to the increase of computational power and research on algorithms and optimization methods, aircraft conceptual design is nowadays carried out by aircraft manufacturers using Multidisciplinary Design Optimization frameworks and sophisticated CAD/CAE software. Currently, many design variables (and types) may be employed, and advanced optimization algorithms that enable complex models of the aeronautical disciplines may be considered. Empirical formulae like the Class-I and -II methodologies proposed by Torenbeek [6] and Loftin [7] for drag and weight estimation are still used because they provide faster results [8]. Because of the increased complexity of such kind of methodology, significant efforts of computational analysis are required to obtain optimum configurations that satisfy many objectives and design constraints.

The extensive investigation of efficient airliners in the 150-250 seating capacity class is the objective of the present work by using an advanced MDO platform, encompassing aircraft which fit into the MMA market segment and their economic feasibility. The optimization tasks properly incorporated an entropy statistics tool for aircraft classification [9] [10]. This tool is based on an unsupervised machine learning algorithm that classifies products into four categories: scaled trajectories (classic); niche; breakthrough, and failure. This criterium was envisaged by Frtenken in his Ph.D. thesis [11]. Aircraft classification was then used as a constraint in the simulations. The multi-objective *gamultiobj* algorithm from MATLAB® was employed in all simulations that were carried out in the present work [12]. Two objectives were considered here: direct operating cost per nautical mile and an efficiency index for the configuration that was elaborated by the authors and will be discussed later in the following sections.

2. Methodology

This Section describes the MDO framework used in the present computations for the tasks to design airliners in the 150-240 seating capacity range. An airplane calculator module is an essential part of this computational tool; therefore, it will be addressed in some level detail. Initially, a description of the entropy statistics module, an important part of the present study, is described.

2.1 Entropy statistics

Historic development and description

German physicist Rudolf Clausius created the entropy concept in 1850 as a thermodynamic property that predicts the irreversibility or impossibility of certain spontaneous processes [13]. In statistical mechanics, entropy is formulated as a statistical property using probability theory. Statistical entropy or entropy statistics (ES) was introduced in 1870 by Ludwig Boltzmann, i.e., the statistical interpretation of the second law of thermodynamics. ES provides a linkage between the macroscopic observation of nature and the microscopic view based on the rigorous treatment of a large ensemble of microstates that constitute thermodynamic systems [13].

Entropy is a physic quantity that measures the degree of system diversity. An important parameter, relative entropy, was introduced by Kullback in 1951 [14]. According to Cover [15], relative entropy is a measure of the distance between two distributions. In statistics, it arises as an expected logarithm of the likelihood ratio. The relative entropy or Kullback-Leiber distance between two probability mass functions p(x) and q(x) is defined by:

$$I(p|q) = \sum\nolimits_{x \in X} p(x) \log\left(\frac{p(x)}{q(x)}\right) \tag{1}$$

Indeed, the relative entropy $I(p|q)$, also known as Kullback–Leibler divergence is a special case of a broader class of divergences called f-divergences, considered a class of Bregman divergences [16]. It is the only such divergence over probabilities that belongs to both classes. Although it is often intuited as a way of measuring the distance between probability distributions, the Kullback–Leibler divergence is not a true metric for this purpose. It does not obey the triangle inequality, and therefore $I(p|q)$ does not equal $I(q|p)$. Nonetheless, it is often useful to consider the relative entropy index as a “distance” between distributions [15]. In its infinitesimal form, specifically its Hessian form, the relative entropy gives a metric tensor known as the Fisher information metric. The relative entropy is always non-negative, and it becomes zero if and only if $p = q$. For applications in the evaluation of product evolution, in Eq. 3, p is a posteriori distribution and q is a priori one. Based on this, two important parameters can be derived, which are important for product categorization. These parameters are called convergence and diffusion. Convergence is obtained when we consider an individual p and look at a certain period in the past and consider the characteristics of another individual q in the same timeframe. For the computation of the diffusion coefficient of a design that appeared in a determined time, designs that appeared after it in a determined timeframe must be selected [9]. Here, we consider the service entry of the aircraft as a time variable. The diffusion of a reference product can then be measured by its distance calculated by Eq. 3 to all the members of the technological population that were selected before. The final I-values are then obtained by dividing the sum of I-values for each product pair by the number of comparisons in the timeframe of observation [14].

The combination of diffusion and convergence indexes is useful for product classification. According to Frenken [9], industrial products can be classified as innovations, scaled trajectories, niches, and failures.

Innovative products can be recognized if they present new, redesigned, or substantially improved characteristics that are well distinguished from their predecessors. Innovative products influence their successors and introduce dominant designs. They are categorized by a low value of diffusion and a high value of convergence indexes. Scaled trajectories or classical designs follow patterns defined by previous concepts and influence their successors. Scaled trajectories are characterized by a low diffusion value as well as a low convergence value.

Products classified as "failures" may even be a market success, as will be shown by the application of the ES tool developed by Ref. [17]. This just means that they did not inherit major characteristics of their predecessors in a stipulated timeframe, and they did not transmit their ones to successors.

Products that fit into market niches are those complying with standards defined by previous designs and do not exert a profound influence on designs that come after them. They may be characterized by the combination of high diffusion and low convergence indexes. Failures are concepts that differ from their predecessors and do not influence their successors, characterized by a high value of its diffusion coefficient and a high value of the convergence index. The kind of design classification of industrial products described before was introduced by Frenken [9]. Figure 3 provides a compilation of this classification. Frenken originally designated designs in the Northeast quadrant as failures. Niche products are in the Southeast quadrant, and the scaled trajectories are in the Southwest one. An ellipse with a center at the confluence of the quadrants defines a region where the configurations are undefined, denominated here fuzzy designs (Figure 3). In the present work, scaled trajectories are referred to as classic airplanes.

Breakthrough products usually feature advanced technology. Sometimes, the creativity employed to define these products rather than technology provides them with unique characteristics. Breakthrough products are intended to fulfill consumer needs to an extended or greater degree than existing products, while most of the time featuring more advanced technology and innovation. These products enjoy the advantage of being the first movers on the market and can establish an early market share lead or a higher market share by outperforming existing products. Although all breakthrough products are first movers, they may not succeed in the marketplace in the long run.

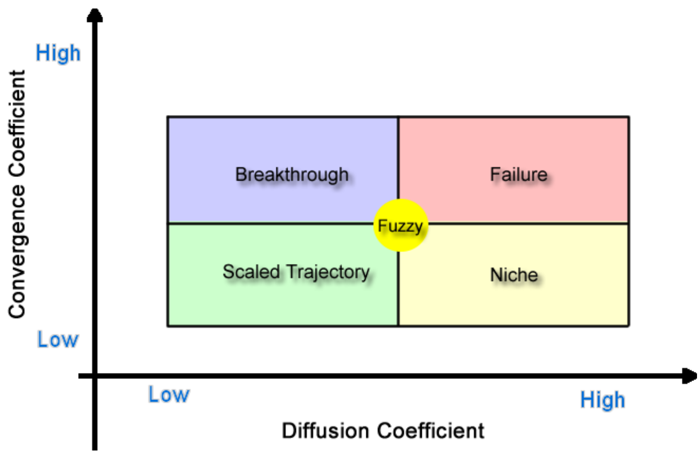

Figure 3: Product classification according to diffusion and convergence indexes

Application to jet airliners market

An Excel worksheet containing data for 123 jet airliners was compiled to feed the code with all data it needs. The first column of the worksheet was filled with airplane names; the second one contains the year of service entry of the airliners. The remaining columns contain the parameters employed for airplane description which are shown in Table 1. Note that the number of airplanes of each type that were delivered is not a variable.

Table 1: Variable stored in the airplane databank for entropy statistics analysis

1) MTOW [kg]	16) Horizontal tail sweepback angle
2) Maximum Zero-Fuel Weight [kg]	17) Takeoff thrust-to-MTOW ratio
3) Operating empty weight [kg]	18) Maximum operating Mach number
4) Fuel capacity [kg]	19) Maximum range with typical passenger payload [nm]
5) Wing reference area [m^2]	20) Service ceiling [ft]
6) Wing aspect ratio	21) Engine configuration (1= two underwing; 2= two at rear fuselage; 3=three at rear; 4= four underwing; 5= four at rear fuselage, 6= two overwing;7=two underwing + one at rear;8=two buried in wing;9=four buried in wing)
7) Wing taper ratio	22) Typical two-class passenger capacity at 32" pitch in the economy class
8) Wing quarter-chord sweepback angle [degrees]	23) Seating abreast in the economy class
9) Passenger cabin external width [m]	24) Wing position (1= low; 2=high)
10) Fuselage length [m]	25) Tail configuration (1=conventional; 2= “T” tail; 3=Cruciform tail)
11) Vertical tail aspect ratio	26) Number of decks
12) Vertical tail taper ratio	27) Number of corridors in passenger main cabin
13) Vertical tail quarter-chord sweepback angle	
14) Horizontal tail aspect ratio	
15) Horizontal tail taper ratio	

Mattos et al. implemented the entropy statistics methodology for product classification [17]. Table 2 contains the classification results for some airliners. Market data for each airplane is also shown in Table 2 to help to evaluate to some extent the degree of success of the airplanes. Most airplanes were properly classified. With the addition of some airliners and the incorporation of more accurate data regarding others, a new classification diagram was generated (Figure 4).

Table 2 – Airliner classification by entropy statistics [17] [18]

Airplane	Year of introduction*	Classification	Units delivered or built*
Boeing 747-400ER	2002	Failure	6
Boeing 767-300ER	1988	Scaled trajectory	583
Boeing 777-200LR	2006	Failure	59
Boeing 777-300	1998	Niche	60
Boeing 777-300ER	2004	Failure	839
Airbus A340-600	2002	Breakthrough	97
Boeing 737-800	1998	Scaled trajectory	4991
Boeing 737-900	2001	Scaled trajectory	52
Boeing 787-8	2012	Scaled trajectory	378
Caravelle VI	1955	Scaled trajectory	109
CRJ-100ER	1992	Failure	47
CRJ-200LR	1996	Breakthrough	298
ERJ145EP/ER/EU/MP	1997	Failure	146
ERJ145LR/LU	1998	Breakthrough	423
ERJ145XR	2002	Niche	110
ERJ135ER	1999	Failure	31
ERJ135LR/LU	2000	Failure/Niche?	94
ERJ140LR	1998	Niche	74
VFW-614	1975	Failure	19
	* Data from Wikipedia and Aifleets.net		

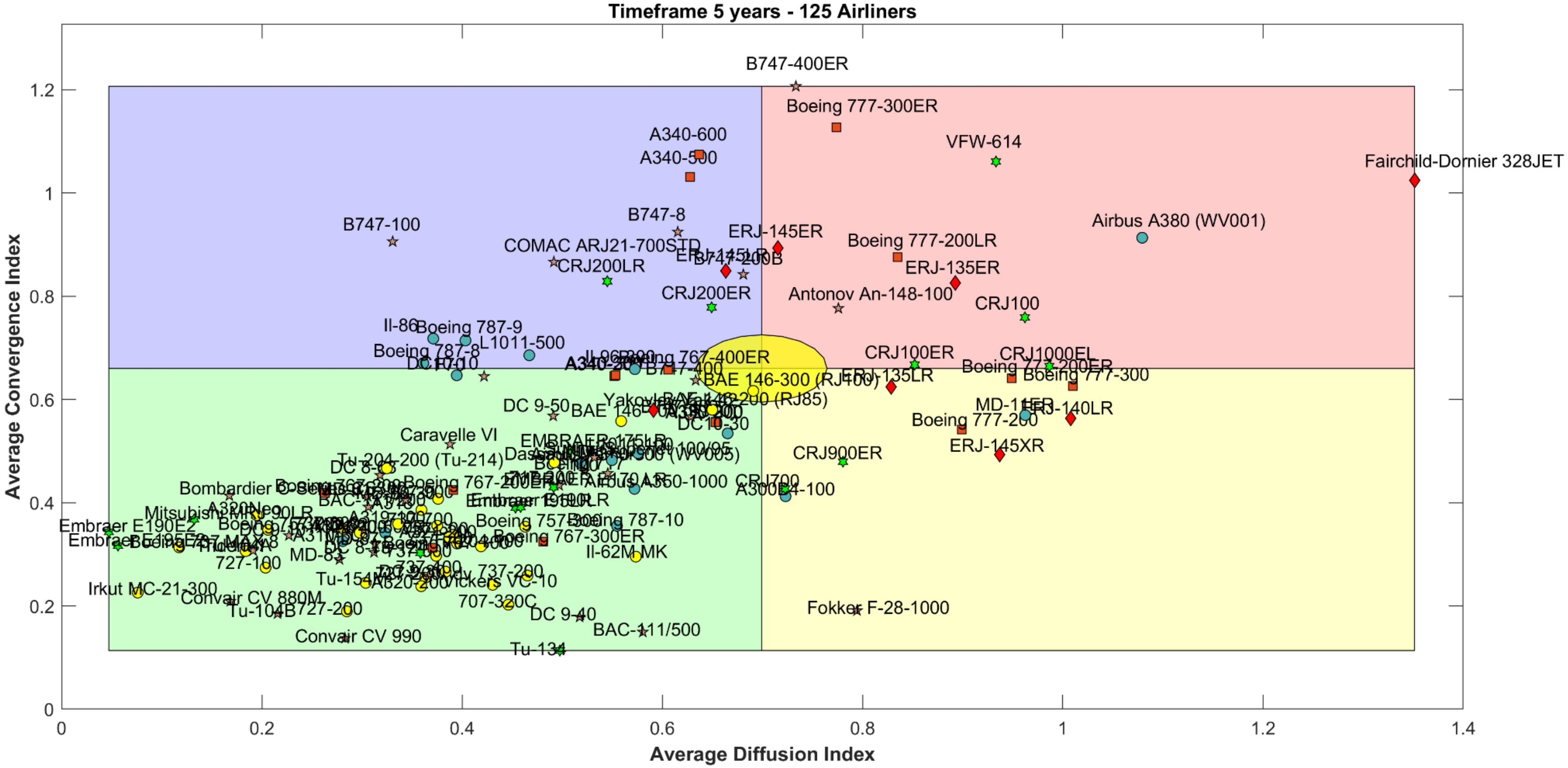

Figure 4: Classification diagram of jet airliners by entropy statistics

The twinjet for 45 passengers EMB-145 found development in the late 1980s. The first concept outlined engines mounted over the wing, which was inherited from the twin-turboprop Brasília. Due to performance issues and a financial collapse of the Brazilian company, the development of the regional jet was lengthened, and the type entered service only in April 1997. By this time the airplane featured rear-mounted engines and the capacity was increased to 50 passengers. Later the type was redesignated ERJ145.

The entropy statistics provided the following results for the three ERJ-145 versions:

- ERJ145ER was positioned in the breakthrough region but remarkably close to that belonging to the failure one. Indeed, this seems to be correct due to the shorter range of this version. The ER was the first ERJ145 version and entered service in 1997. Embraer soon perceived this shortcoming and quickly developed and offered the LR version with a greater range, already in 1998.
- ERJ145LR. This version was labeled as a breakthrough design which also seems to be correct. Its direct competitor, the CRJ100 twinjet, entered service considerably earlier, in 1992. The CRJ 100 presents a range of 1,000 nm with a payload of 50 passengers; while the CRJ 100ER had its range increased to 1,650 nm with the same payload [19]. Why the Canadian CRJ 100 was not also categorized as a breakthrough? This can be possibly credited to its shorter range and heavier MTOW (23,133 kg). Probably in this category, the ERJ145LR seems to present the right characteristics to be classified as a breakthrough. Bombardier introduced the CRJ-200LR in 1996 [20], which features a 1,800-nm range (50 PAX) and better airfield performance when compared to the -100ER version. Alongside the ERJ145LR, the CRJ-200LR airliner appears in the classification box as a breakthrough concept.
- ERJ 145XR. This airplane seems to have been designed to fulfill a market niche. This version of the ERJ 145 presenting improved performance was purchased by ExpressJet (former Continental Express) only, a subsidiary of Continental Airlines. The Newark airport was the main operational base for this type. Thanks to the better performance when compared to the LR version, the ERJ 145XR enabled ExpressJet to service more distant cities from Newark.

For the high-capacity market, the classification that resulted for the B777-300ER and the A340-600 provides good stuff for discussion. Boeing B777-300.

- The long-haul A340-600 airliner can transport 361 passengers for a 7,540 nm stage length. This performance is comparable with that of B777-300ER when accommodating 339 passengers in a typical two-class layout (Figure 5). The A340-600 entered service in 2002 and the B777-300ER two years later [21]. Although with a poor sales record, the A340-600 was categorized as a breakthrough and its direct competitor as a failure. According to Table 2, the B777-300ER presents an outstanding sales record. It is worth mentioning that a breakthrough design is not a synonym for a successful product, therefore it could be a failure. On the other hand, regarding the B777-300ER airplane, based on the fundaments of ES its classification makes sense because, in the timeframe of 5 years (and even longer), there is no other similar airplane to the B777-300ER. Thus, it received the "failure" label. The question that could be placed here is why the A340-600 was not as successful as the Boeing airplane. This probably resides in the number of engines; airlines prefer twin-engine airplanes for easy maintenance and maintainability.

- Launched in June 1995, the Boeing 777-300 major assembly started in March 1997, and it was rolled out on September 8 and made its first flight in October. The B777-300 was designed to be stretched accommodating 451 passengers in two classes, or up to 550 in an all-economy like the 747SR. Contrary to the extended range version, its sales record is not successful, indicating that airlines preferred the range instead of the larger capacity. It was classified as a niche by the ES application.

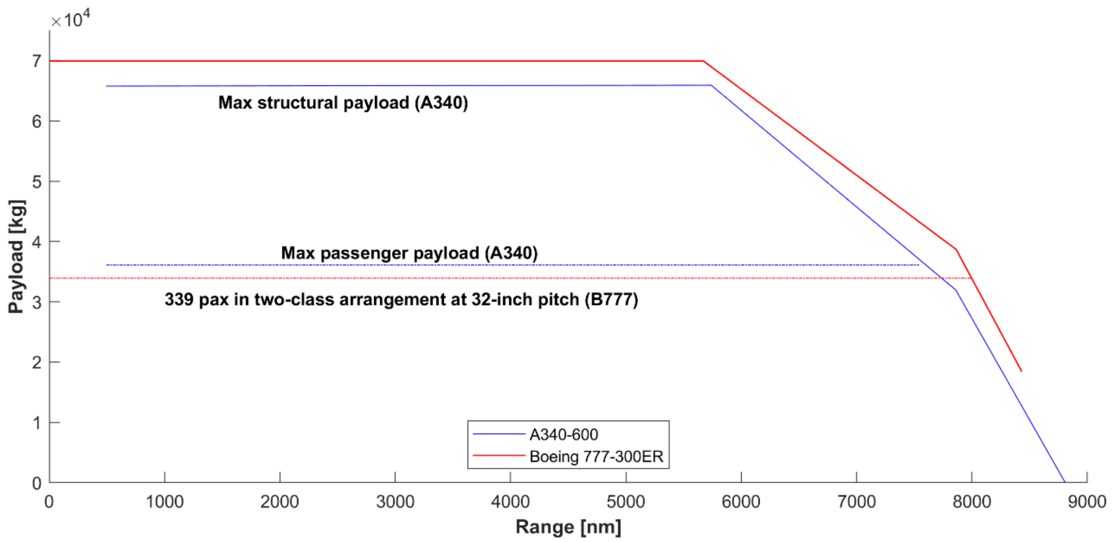

Figure 5: Payload-range diagrams for A340-600 and B777-300ER [22] [23]

Classification tree

The Classification Tree Method is a method for test design, as it is used in different areas of product development. It was elaborated by Grimm and Grochtmann in 1993 [24]. Classification Trees in terms of methodology cannot be confused with decision trees.

Classification tree methods greatly enhance the analysis capability the way of considering survey data and other information into it. There are three methods for producing classification trees: AID (automatic interaction detection), CHAID (chi-squared automatic interaction detection), and CHAID/CART (CHAID and classification and regression tree).

The classification tree method consists of two major steps:

- Identification of test-relevant aspects (so-called classifications) and their corresponding values (called classes) as well as
- Combination of different classes from all classifications into test cases.

The identification of test-relevant aspects usually follows a functional specification of the system under evaluation. These aspects form the input and output data space of the test object. The second step of test design follows combinatorial test design principles.

The chi-square automatic interaction detection (CHAID) is currently the most popular classification tree method. CHAID is much broader in scope than AID and can also be applied when the dependent variable is categorical. The algorithm that is used in the CHAID model splits records into groups with the same probability of the outcome, based on values of independent variables. Branching may be binary, ternary, or more.

When the relationship between a set of predictor variables and a response variable is linear, methods like multiple linear regression can produce accurate predictive models. However, for a system highly non-linear and complex, methods to handle non-linear behavior is a must. One such example of a non-linear method is classification and regression trees, often abbreviated as CART. As the name implies, CART models use a set of predictor variables to build decision trees that predict the value of a response variable.

Regarding node splitting rules, the MATLAB® command *fitctree* uses these processes to determine how to split node t [25]. For standard CART and for all predictors $x_i = 1, \ldots, p$:

- *fitctree* computes the weighted impurity of node t, i_t.
- *fitctree* estimates the probability that an observation is in node t using

$$P(T) = \sum_{j \in T} w_j \tag{2}$$

with w_j being the weight of observation j, and T is the set of all observation indices in node t. If you do not specify prior or weights, then $w_j = {}^{1}/_{n}$, where n is the sample size. There are additional important rules that are available in Ref. [25].

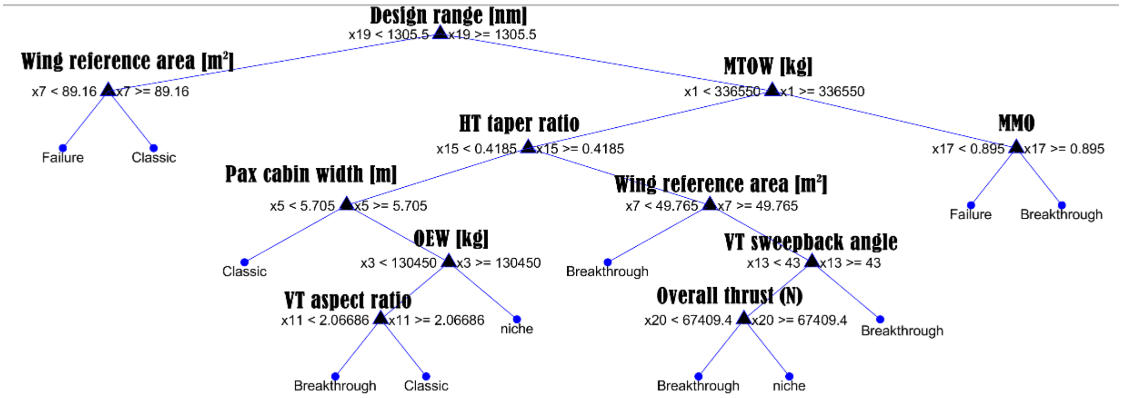

Figure 6: Decision tree classification based on ES

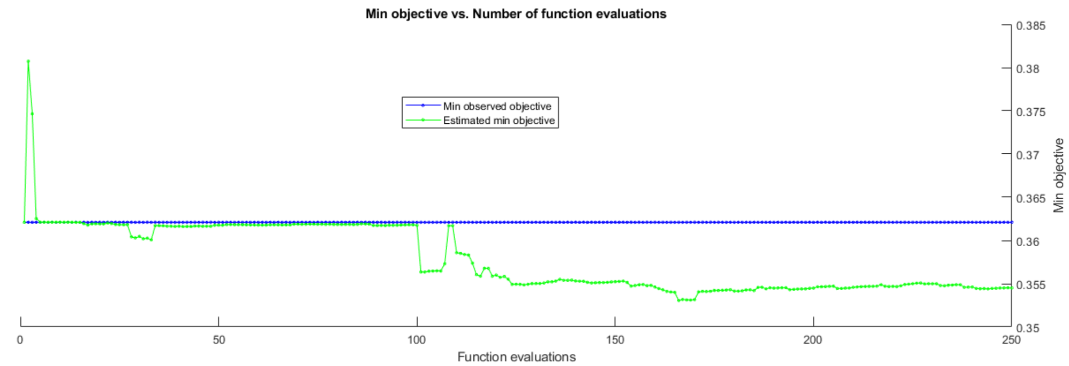

Figure 7: Convergence log of the Bayesian optimization task

The *fitctree* MATLAB® command was used to construct the tree seen in Figure 6. The convergence process with a Bayesian optimizer can be seen in Fig. Y. *fitctree* generates a classification tree model that can be an input for a predictor algorithm that delivers a label. Data of some airplanes already classified by ES were input into the predictor algorithm. Their labels of the classification tree were the same as those provided by ES.

It was expected that the configuration variables (see Table 1) would be part of the tree in Figure 6, mainly related to engine configuration. On the other hand, the appearance of the VT sweepback angle could be an indication that the classification tree of Figure 6 needs great improvements and is not ready to be employed in simulations, as a surrogate of the ES method. This utilization would be very interesting, considering that saving in computational cost will be considerable and the surrogate would deliver a classification independent of the time of aircraft service entry.

Dendrogram

Dendrograms are a good tool for group products, and they fit into the hierarchical clustering category [26]. MATLAB® has some algorithms that are easily able to compose a dendrogram. Considering the information shown in Table 1 and normalizing it, the Euclidian distance is calculated between all airliners from the databank, and then the Dendrogram is built (**Fig. 4)**. This figure reveals the 10 closest configurations to the 767-200 high-gross sub-version (MTOW of 115,650 kg [27]). The cluster analysis using the Dendrogram approach correctly identified the larger 757-300 version as the closest configuration to the Boeing 757-200 airplane. Airbus A321-200 and a variant A321LR were placed in a group that is remarkably close to Boeing's airplane. Thus, this tool was then certified to be used for finding out individuals in the Pareto front closest to any reference airplane of choice, such as the Boeing 757-200.

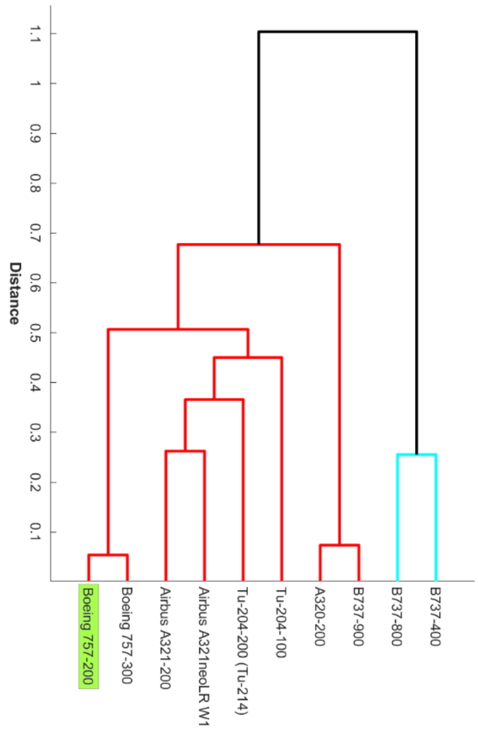

Figure 8: Dendrogram plot of the closest airplanes to Boeing 757-200

2.2 Optimization approaches

Thanks to the increase in computational power and advanced algorithms, and optimization methods, aircraft conceptual design is nowadays carried out by aircraft manufacturers using multi-disciplinary design and optimization frameworks and sophisticated CAD/CAE equipment. A great deal of computational analysis is required to obtain optimum configurations to satisfy many objectives and design constraints. Disciplines such as aerodynamics, propulsion, flight mechanics, structures, and aeroelasticity, among others, are frequently considered in the optimization framework to obtain more realistic geometries of flight vehicles and, recently, the addition of flight profiles and mission analysis [28]. Nowadays, many design variables (and types) may be employed, and advanced optimization algorithms that enable complex models of the aeronautical disciplines may be considered. Empirical formulae like the Class-I and -II methodologies proposed by Torenbeek [6] and Loftin [7] for drag and weight estimation are still used because they provide faster results [8]. Because of the increased complexity of such kind of methodology, significant efforts of computational analysis are required to obtain optimum configurations that satisfy many objectives and design constraints.

CFD analysis of complex aircraft configurations is still time-consuming, thus hampering in part its application in aircraft conceptual and preliminary design. Aerodynamic analysis requires considerable computational resources and labor work for the construction of complex 3D computational meshes, necessary to produce credible results. The case is even worse for multi-disciplinary optimizations, which deal with high-dimension problems that may reach thousands of design variables and their relationships. However, surrogate techniques have been increasingly adopted to model the physics with enough precision and at the same time reduce the computational time of complex and heavy calculations in MDO frameworks [28] [29].

The use of gradient-based optimization algorithms associated with adjoint methods is an alternative to cut considerably the processing time of optimization problems since their computational cost does not strongly scale up with the number of design variables compared to evolutionary algorithms [30]. “There are two approaches for the adjoint method: continuous adjoint, by deriving the exact adjoint equation and then linearizing it; or the discrete adjoint, by directly deriving it from the discretized flow equations” [30]. “Both approaches compute the adjoint variables by an additional linear system of equations. Afterward, together with the mesh sensitivities, the final sensitivities, or gradients, are evaluated and transferred to an optimizer” [30].

On other hand, there are some limitations of the adjoint methodology:

- Huge and long tasks must be carried out in preparation for several third-party codes to be used for automatic differentiation algorithms (Their source codes sometimes are not available).
- Usually, mono-objective optimization for aircraft conceptual design is possible. For objectives encompassing several disciplines, the approach employed by adjoint optimization frameworks is to proceed with a weighted sum of objectives.
- It is challenging to consider optimization problems with discrete variables.
- It is characterized by low flexibility in changing constraints and objectives.
- Adjoint methods can handle tens of thousands of variables to define a wing geometry. However, airfoil geometry can be defined by ten or a few more variables by using parametrization like PARSEC [31]. **Fig. 12** illustrates the excellent modeling capability performed for the NACA21010 airfoil by a PARSEC parametrization with just 12 parameters.

Genetic algorithms, an evolutionary approach based on their metaheuristic of reproduction of the fittest, have widespread and effective use in the optimization of aircraft configuration [32] [33]. The procedure of reproduction of the fittest is repeated until some established criterium to close the process is reached. Evolutionary algorithms solve both constrained and unconstrained optimization problems its great advantage lies in the absence of the necessity of gradient calculation of the objective function with regards to the design variables. Opposed to this, is that this necessity is present in classic gradient optimization methods such as gradient descent and quasi-newton methods.

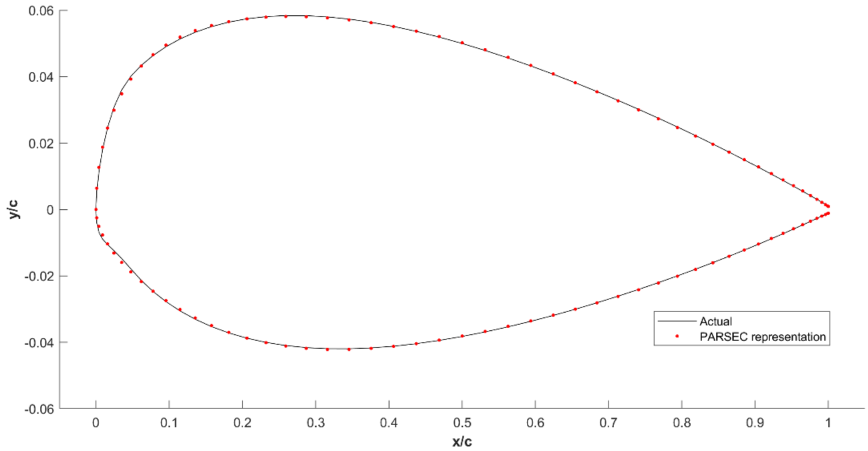

Figure 9: PARSEC representation of NACA21010 airfoil

Bayesian optimization is another approach that offers advantages over the adjoint and heuristics methods. It employs a sequential design strategy for global optimization of black-box functions that does not assume any functional forms. Bayesian optimization is usually employed to optimize expensive-to-evaluate functions [34] [35]. Since the objective function is unknown, the Bayesian strategy is to treat it as a random function and place a prior over it. The prior captures confidence about the behavior of the function. After gathering the function evaluations, which are treated as data, the prior is updated to form the posterior distribution over the objective function. The posterior distribution, in turn, is used to construct an acquisition function (often also referred to as infill sampling criteria) that determines the next query point.

Priem et al. [34] employed Bayesian optimization for the optimal design of a business jet (BJ) designated Bombardier Research Aircraft. Conceptual and preliminary design thee addressed with the Bayesian optimization approach. For the conceptual design, 11 design variables were selected, with 6 of them related to rear spar chordwise location and airfoil maximum relative thickness along definition stations along the wingspan.

The constrained Bayesian optimization procedure is summarized below:

Problem setup: objective and constraints functions, starting D0E and setting the maximum number of iterations
Loop i=1 to max iterations
Build the surrogate models using Gaussian Process
Find x^{i+1} a solution to the enrichment maximation sub-problem
Evaluate objectives and constraints
Update de DoE
End loop
Final solution: the optimal point from DoE

2.3 Robust Optimization

Robust optimization (RO) has undoubtedly become an effective method of choice for optimization under uncertainty in process systems engineering with practical applications ranging from production scheduling to airfoil and wing design. RO does not presume that probability distributions are known, but instead, data uncertainty ordinarily resides in a user-specified set of uncertain parameter values, called the uncertainty set [36]. In RO the modeler aims to find decisions that are optimal for the worst-case realization of the uncertainties within a given set. Typically, the original uncertain optimization problem is converted into an equivalent deterministic form, called the robust counterpart, using strong duality arguments and then solved with standard optimization algorithms.

However, robust optimization methodologies have an important drawback. By the very nature of the methodology, robust optimal solutions are highly conservative, aiming to hedge against all possible worst-case realizations of the uncertainty. In some cases, this can lead to solutions that are too conservative. For example, if a chemical plant or biorefinery is designed too conservatively, then the project may be too expensive or needlessly complex. Researchers have looked for methods to control the robustness or conservativeness of robust optimization techniques, and some promising methods, such as adaptive or adjustable robust optimization have recently surfaced.

The main techniques of robustness used to solve optimization problems with uncertainty are summarized as follows [37]:

- *Strict robustness or static robustness*. Static RO intends to find solutions that are resistant to all perturbations of the data in a so-called uncertainty set. First, consider that $x \in S$ is a solution to the optimization problem with uncertainty $P(\xi)$, with $\xi \in U$. The solution is strict if x is feasible for all possible scenarios of U, that is if $F(x, \xi) \leq 0$ for all $\xi \in U$. This technique is very intuitive to solve the optimization problem robustly.
- *Cardinality constrained robustness*. One approach to relaxing the strict robustness is to restrict the space of uncertainty. This way, it allows for accounting for a certain degree of uncertainty with a reasonable computational effort, providing a trade-off between computational time and robustness. In addition, it can be tuned to consider the specific degree of risk the decision maker accepts [38].
- *Light robustness*. A completely different way of relaxing the concept of strict robustness corresponds to instead of reducing the space of uncertainty, we can relax the constraints in favor of the quality of the solution.
- *Adjustable robustness*. Another way to relax the space of uncertainty of strict robustness is to split the space into groups of variables. In this technique. some of the decision variables are adjusted after some portion of the uncertain data reveals itself [36].
- *Recoverable robustness*. Recoverable robustness uses the concept of a recovery algorithm, and, like adjustable robustness, it obtains the solution in two stages. Give a family of algorithms A. A solution x is recovery robust concerning A if it exists for every scenario $\xi \in U$, an algorithm A applied to the solution x, and a scenario ξ allows you to build a solution $A(x, \xi) \in F(\xi)$ [37].

2.4 Airplane analysis tool

Introduction

The airplane analysis tool (AAT) is the masterpiece of the present design framework. It provides an embracing description and characterization of the airplane. Many levels of fidelity for discipline representation are available. AAT also calculates the noise and emissions footprint. Detailed mission performance and range evaluations are derived from flight profiles set by the user and obeying air traffic constraints, all based on the aerodynamics, mass, and engine characteristics of the airplane. It is possible to examine any design mission or off-design missions corresponding to specific takeoff weights or required block distances.

The airplane mission setup is highly detailed with a flight profile that makes accurate calculations of major airplane masses possible like MTOW, OEW, and MZFW. Air traffic constraints can be incorporated into the calculation, if required [39]. Several aerodynamic methods are available in the framework with different levels of fidelity, including an artificial neural network surrogate model, which is the object of the present work. An in-house generic turbofan engine model is also part of the MDO framework [40]. It is possible to analyze the performance, emissions, and operational costs for missions inside a complex airline network with different takeoff weights or block distances [41]. The fuel storage capacity is precisely calculated considering the actual airplane geometry and structural layout.

All mission segments are analyzed, and optimal and transitional climb altitudes are calculated considering buffet margins, available engine thrust, rate of climb, and accurate airplane lift-to-drag ratio. Alternate airport, hold and descent patterns, reserve and maneuvering fuels, and weight allowances are additional parameters. Typically, after the second segment climb, the in-route climb uses airspeed schedules, namely, a calibrated airspeed (CAS) segment followed by a constant previously stipulated Mach number until the initial cruise altitude. The cruise phase can be flown at a constant altitude or following a step-increasing altitude pattern. There are two cruise speed profiles, one with a constant Mach number, the other being a long-range pattern.

Fuel storage

Fuel is stored in the wingbox and there is a routine that computes the available volume, and therefore it requires information on wing spar location. Depending on user choice, fuel can also be stored in a fuel tank located inside the fuselage close to the position where the wing-fuselage junction is.

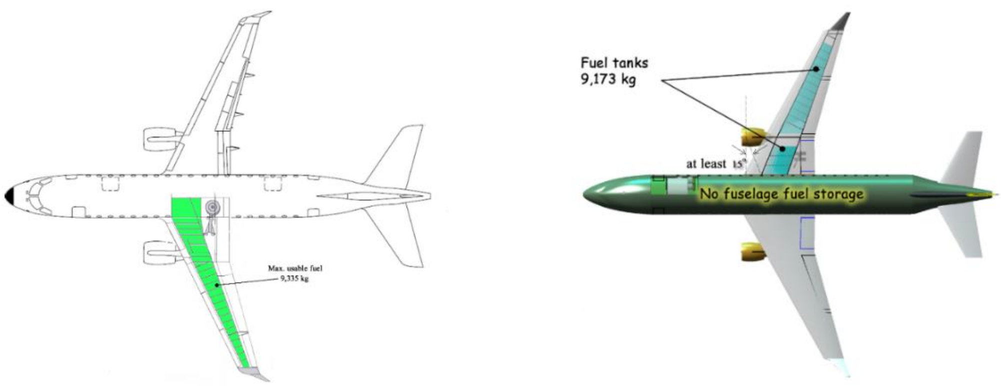

Figure 10: Fuel storage in actual aircraft (on the left) and for the model of the present work (on the right)

For purposes of illustration, the fuel storage approach of Embraer E-jets is depicted in **Fig. 5**. Besides the storage inside the wing, another region where the fuel can optionally be stored is a place inside the fuselage. It is worth mentioning that the boundary of the wing outboard tank is close to the wingtip [42]. According to the manufacturer, the E170 has a usable fuel capacity of 9,428 kg. The airplane analysis tool offers two options already outlined before: the first one considers that the fuel is stored only in the wings and the tanks extend until 90% of the wingspan (**Fig. 5**). In this case, for the E170, the resulting fuel capacity is 9,178 kg. As the airfoil geometry for this twinjet is not available, this figure is just an approximate value; the other possibility in the design framework is to consider a fuel tank inside the fuselage. Its capacity is then dependent on the cabin's central fuselage dimensions and the location of the cabin floor.

Maximum lift coefficient

High-lift characteristics have a huge impact on the sizing, economics, and safety of an airplane. Airplanes featuring lower approach speed are safer and complex high-lift systems increase manufacturing costs and reduce flight dispatchability. It is important to achieve the highest possible maximum lift coefficient at takeoff and landing to avoid the necessity of higher wing areas.

Applied analysis of the Navier-Stokes equations is very time-consuming due to the complex nature of the flow in combination with complex geometries. In addition, considering regions of highly separated flow convergence of the solution poses an immense difficulty for the code. Several analytical methods that both account for stall effects and enable the prediction of the maximum lift coefficient were discussed and a trade-off between the methods was conducted in Ref [43]. From this trade-off, it was found that both the pressure difference rule and the so-called Critical Section Method are good options in terms of accuracy and versatility.

The pressure difference rule, on the other hand, determines wing stall by implementing an empirical chordwise pressure difference criterion. Thus, wing stall is established when the wing section's chordwise pressure difference, at an angle of attack, equals the critical pressure difference which is empirically derived and depends on both the Mach- and Reynolds number.

The critical section method utilizes a two-dimensional airfoil analysis code for the maximum lift coefficient calculation at many prescribed wing sections. By using three-dimensional wing-fuselage combinations C_{L0} and $C_{L\alpha}$ coefficients for the wing sections are obtained. After a sweeping procedure, a stall is reached when the lift coefficient distribution along the semispan is locally equal to the wing section's maximum lift coefficient.

Singh [43] validated both the pressure difference rule and critical section method against wind-tunnel experiments, both for wing-only samples and wing-fuselage configurations. The approximation of the clean maximum lift coefficient showed to be in good agreement, with about a 3% error margin, which is a particularly good figure.

For the present computations, a MATLAB® code was elaborated to automatically run the panel code XFOIL [44] for the calculation of section maximum lift coefficient. A full potential code for wing-fuselage combinations then calculates the lift coefficient distribution along the wingspan at two conditions with different angles of attack. After the clean wing configuration is calculated, the Datcom method [45] is used to estimate the maximum lift coefficient at takeoff and landing from flap configuration and some wing geometric parameters.

Empty weight calculation

For the calculation of the maximum takeoff weight (MTOW), the estimation of the empty weight is needed, which can be supplied according to the MTOW (class I weight method) itself or it can be calculated by the sum of the individual structural weights and aircraft systems (class II method). Within the Class I methodology, the following relationship between MTOW and OEW was developed by the authors:

$$\frac{OEW}{MTOW} = \left[a + b\left(\widehat{MTOW}\,\widehat{AR}\,TW\,\widehat{S_w}\,MMO\,\hat{L}_f\,F_w\hat{\Psi}\,\widehat{SC}\right)^{C0} + c\left(\widehat{MTOW}\right)^{C1}\left(\widehat{AR}\right)^{C2}(TW)^{C3}\left(\widehat{S_w}\right)^{C4}(MMO)^{C5}(\hat{L}_f)^{C6}(F_w)^{C7}(\Psi)^{C8}(\widehat{SC})^{C9}\right] \quad (3)$$

Eq. 3 was tailored for a mix of units of the international and English systems. The MMO, TW, and F_w symbols refer to the maximum Mach of operation, the thrust-to-weight ratio, and the diameter of the cross-section of the passenger cabin, respectively.

Normalizations that were considered in **Eq. 3**, are given in Table 3.

Table 3: Variable normalization for Eq. 3

$\widehat{MTOW} = \frac{MTOW}{50000}$	$MTOW$ = Maximum Takeoff Weight [kg]
$\widehat{AR} = \frac{AR}{8}$	AR = Wing aspect ratio
$\widehat{WL} = \frac{WL}{100}$	WL = Wing loading [kg/m^2]
$\hat{L}_f = \frac{L_f}{30}$	L_f = Fuselage length [m]
$\hat{\Psi} = \frac{\Psi}{20}$	Ψ = Quarter-chord sweepback angle [degree]
$\widehat{SC} = \frac{SC}{40000}$	SC = *Service Ceiling* [ft]

Table 4: Values of the coefficients present in Eq. 3

a	b	c	C1	C2	C3	C4	C5	C6	C7	C8	C9
-0.2359	-0.3065	0.8900	-0.1731	0.0871	0.0857	0.1050	-0.0931	0.1220	0.2232	0.0857	0.0418

To obtain the exponents and multipliers of the terms of **Eq. 3**, the authors used a database of line aircraft containing information from 123 models, with entry into service from the 1950s to others with commercial operation expected in 2020. **Fig. 6** shows the relationship between the MTOW and the reference area of the wings for the aircraft in the database. An optimization algorithm was elaborated for the minimization of the mean quadratic error between the OEW/MTOW estimated by **Eq. 3** and the actual values of the airplanes in the database. The exponents and coefficients of **Eq. 3** are the design variables. The mono-objective genetic algorithm of MATLAB® 2019a was used in optimization simulations and after 5500 generations the simulation was stopped. Table 4 shows the coefficients and exponents that the optimization run provided. Table 5 contains some estimation errors for the weight fraction.

Table 5: Estimation error of weight fraction for some jet airliners

Airplane	Actual OEW/MTOW	Calculated OEW/MTOW	Percent error
Boeing 737-700	0.54157	0.53548	1.12
Airbus A320-200	0.54494	0.53829	1.22
B747-400	0.49077	0.4976	1.39
Boeing 757-300	0.53874	0.49639	7.86
Boeing 767-300	0.55681	0.55400	0.505
CRJ200ER	0.59806	0.59552	0.425
EMBRAER E170LR	0.55645	0.56798	2.07
Fokker 100	0.57074	0.55416	2.90
Tupolev Tu-104A	0.54737	0.56043	2.39
VFW 614	0.61048	0.60329	1.18

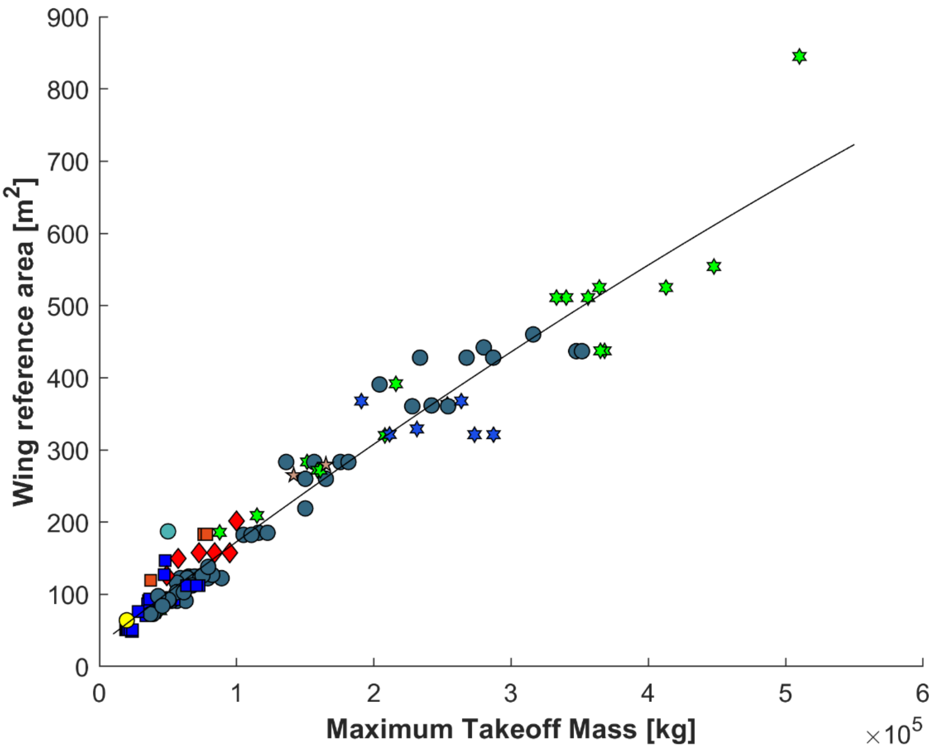

Figure 11: MTOW plotted against wing reference area considering airplanes utilized for the elaboration of Eq. 2. The different symbols in the graph reflect the different engine configurations

Engine weight calculation

There are some simple methods as well as some more sophisticated methods for the estimation of turbofan engine weight [46]. But for WATE++, all of them are not accurate enough to be used in the optimization framework for airplane design. Thus, a methodology developed by the authors was adopted for turbofan engine weight estimation. This approach utilizes a formulation based on some engine geometric and thermodynamic parameters (**Eq. 4**).

$$W_E = \frac{T1 * (BPR/\overline{BPR})^a (OPR/\overline{OPR})^b (T_s/\bar{T})^c (D_E/\overline{D_E})^d (L_E/\overline{L_E})^e (\dot{m}/\bar{\dot{m}})^f +}{T2 * (BPR/\overline{BPR})(OPR/\overline{OPR})(T_s/\bar{T})(D_E/\overline{D_E})(L_E/\overline{L_E})(\dot{m}/\bar{\dot{m}}) + T3} \quad (4)$$

The coefficients and exponents of **Eq. 3** were obtained by optimization using a genetic algorithm [47]. The objective was the minimization of the square mean error of known engine weights. A database, comprised of 20 engines, was elaborated which embraced a large variety of turbofan engines [48]. Table 6 shows the coefficients and A, B, and C parameters obtained with the optimization process. Table 7 shows the average parameters used for normalization in **Eq. 4**.

Table 6 - Obtained exponents and coefficients for Eq. 4

Coefficient/exponent	Value
T1	2587.2461
T2	50.1920
T3	154.6179
a	-0.1965
b	-0.0718
c	1.0435
d	0.2493
e	-0.3444
f	-0.1455

Table 7: Parameters used for normalization in Eq. 4

Parameter	Value
$\overline{BPR}$	4.6911
$\overline{OPR}$	25.4000
$\bar{D}_E$ [m]	1.7906
$\bar{L}_E$ [m]	3.3276
$\bar{T}$ [kN]	148.1217
$\bar{\dot{m}}$ [kg/s]	464.7333

Table 8 contains weight estimation errors for some known turbofan engines.

Table 8: Weight error estimation for some known engines

Engine	Percent error
AE3007A1P	10.94
CF6-50C	2.55
JT8D-219	0.74
GE CF-34-10A	6.48
R&R RB211-535C	0.97
Trent 800-875	3.12
Williams FJ-44	4.29
Pratt & Whitney PW2040	0.44
GE-90/77B	0.31
R&R Tay 620	2.65

Workflow of the airplane analysis tool

The airplane calculator workflow is shown in Figure 12. From airplane geometry and topology an iterative process for MTOW calculation is performed. The formulation for the OEW/MTOW weight fraction of **Eq. 3** and the methodology outlined in **Eq. 4** for the estimation of the engine weight is employed in this process. To evaluate the accuracy of the present design workflow three airliners of different categories were analyzed and **Tables VIII-XI** contain their characteristics and those estimated by the airplane calculator tool.

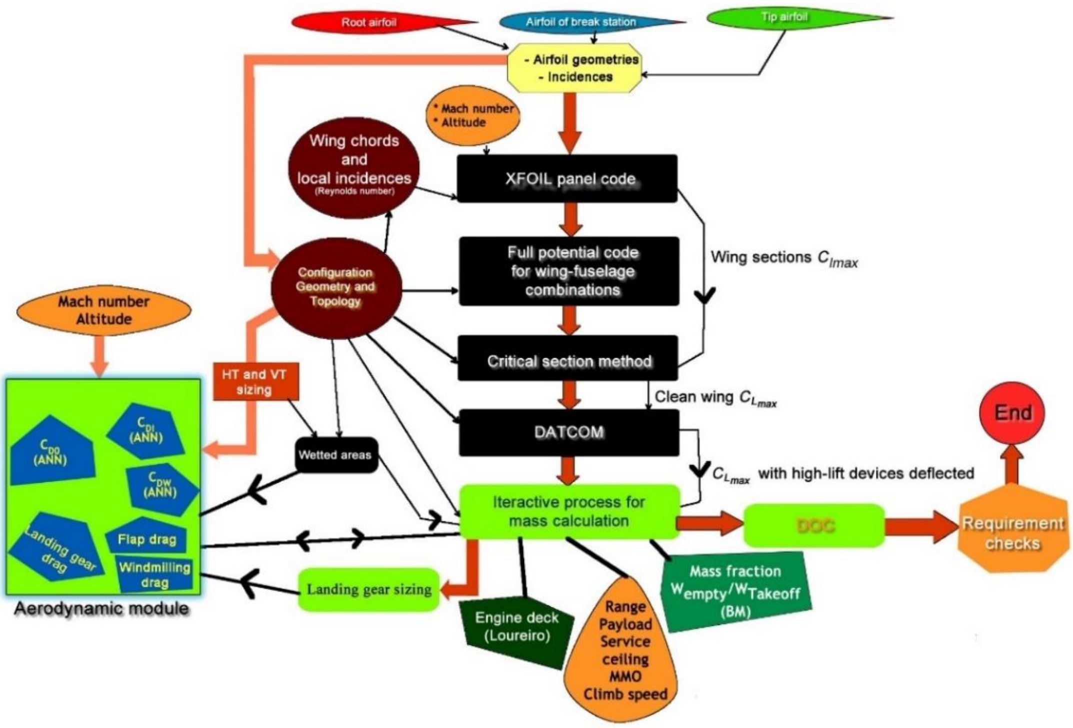

Figure 12: Workflow of the airplane analysis tool

Calculating the A320 airliner

The A320 twinjet presents a six-abreast cross-section and is powered by either CFM56 or IAE V2500 turbofans. The A320 family, which includes the A318 and A321, pioneered the use of digital fly-by-wire and side-stick flight controls in airliners. Variants offer maximum take-off weights from 68 to 93.5 t, to cover a 5,740–6,940 km (3,100–3,750 nm) range [49]. Some of the A320 main characteristics are presented in Table 9 and the MTOW and OEW calculated by the present methodology are given in Table 10**.**

Table 9: Characteristics of A320-200

Design Range	L_f	wAR	wS	wSw14	BPR	Engine Dry Weight	D_E
$2,350^{\alpha}$ nm	37.57 m	10.33	122.4 m^2	25º	4.8:1	2,400 kg	1.75 m
MTOW	**OEW**	**Usable fuel**	**T**	**Aisle Width Y-class**	**MMO**		
$73,500^{\theta}$ kg	$42,600^{\Psi}$ kg	$21,005^{\beta}$ kg	220 kN	0.48 m	0.82		
α @ FL370, a payload of 15,000 kg, ISA+0 ºC, takeoff with MTOW, IAE V2500-A5							
β Includes one fuselage tank							
θ Airbus A320-200 WV015 [50]							
Ψ Ref. [51]							

Table 10: Estimated values for the A320-200 airliner by the present design framework

MTOW	OEW	Fuel Capacity	Range	Categorized as
73,440 kg	41,371$^{\alpha}$ kg	19,795$^{\alpha}$ kg	2,350 nm $^{\alpha}$	Classic
α @ FL370, a payload of 15,000 kg, ISA+0 ºC, takeoff with MTOW, IAE V2527-A5, 200 nm to an alternate airport				

The B757 has a six-abreast cross-section and is powered by either RB211 or PW2030 and PW2040 Series turbofans. The B757-200 is the basic version, which entered service in 1983.

In August of 1978, Eastern Airlines and British Airways announced orders for the B757 and chose the RB211-535 to equip the airplane [52]. Designated RB211-535C, the 3-spool engine entered service in January of 1983 when the first B757-200 was delivered to Eastern Airlines. The engine has a nominal thrust of 37,400 lbf (166.36 kN) and an OPR of 21.2:1 [53]. In 1979, Pratt & Whitney launched its PW2000 engine, claiming 8% better fuel efficiency than the -535C for the PW2037 version [52]. The English engine manufacturer reacted and using the -524 core as a basis, the company developed the 40,100 lbf (178 kN) thrust RB211-535E4, which entered service in October of 1984. There are differences in appearance between the two versions like a mixed exhaust nozzle and a bigger fan cone for the RB211-535E4. BPR was slightly reduced to 4.40:1 from 4.46 for the 535C [53]. There is another version of the Rolls&Royce engine designated RB-211E4B, which has a takeoff thrust of 43,500 lb [54]. The 535E4 engine was also the first to use the wide chord fan which increased efficiency, reduced noise, and gave increased protection against damage from foreign object ingestion [52]. As a result, a relatively small number of -535Cs was installed on production aircraft in May of 1988. American Airlines ordered 50 B757s powered by the -535E4 emphasizing the engine's low noise as an important factor in their choice. The stretched version B757-300 entered service with Condor Flugdienst in 1999. With a length of 54.5 m, the type is the longest single-aisle twinjet ever built.

According to Ref. [27], The B757-200 has several sub-versions presenting different MTOW, OEW, and MZFW. Two configurations fitted with RB211-535E4B engines were selected as references for the present work, and their payload-range diagrams are shown in Figure 13 and some characteristics are given in Table 11 [54]. Two ranges signaled by the dashed lines in the payload-range diagrams are related to a mission with a payload of 192 passengers.

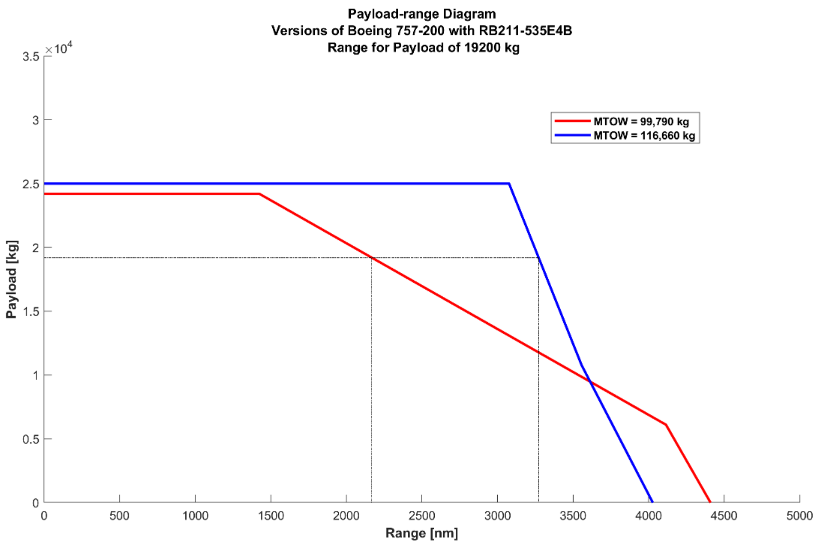

Figure 13: Payload-range diagram for some sub-versions of B757-200 [54]

Table 11: Characteristics of two B757-200 sub-versions fitted with RB211-535E4B engines [22] [54] [53] [52]

Sub-version	MTOW	OEW	MZFW	Usable fuel	Takeoff Thrust	TFL
1	99,790 kg	58,570 kg	83,460 kg	42,680 kg	37,400 lbf	1,660 m
2	115,650 kg	58,570 kg	84,360 kg	43,490 kg	43,500 lbf	2,070 m
L_f	wAR	wS	wSw14	MMO	Aisle width of Y-class	
46.97 m	7.82	185.25 m^2	25º	0.86	0.508 m	

Some of the B757-200 main characteristics calculated by the present methodology are given in Table 12. Again, the agreement between actual and estimated weights is particularly good. The year 1984 was set for the year of service entry. As expected, the airplane was categorized as a classic design (scaled trajectory). However, just for testing, if the year 1981 were adopted for that parameter, the airplane would be labeled by the entropy statistics classification program as a breakthrough, as also is expected. The reason behind this is simple: this way the configuration being analyzed passes its unique characteristics to the actual airplanes that entered service in 1983 and 1984, which are part of the database.

Table 12: Characteristics of B757-200 model fitted with RB211-535E4

MTOW	OEW	Fuel Capacity	Range	Categorized as
115,100 kg	58,495$^{\alpha}$ kg	41,138$^{\beta}$ kg	3,272 nm$^{\alpha}$	Classic
α @ FL370 and FL390, Mach of 0.80, payload of 19,200 kg, ISA+0 ºC, takeoff with MTOW, RB211-535E4, 200 nm to an alternate, 30 min loiter @ 1,500 ft				
β wing capacity of 30,918 kg / ε Jet A1 price of US$ 2.387 US$/gal				

2.5 Multi-disciplinary and multi-objective optimization

Introduction

Thanks to the increase of computational power and research on algorithms and optimization methods, aircraft conceptual design is nowadays carried out by aircraft manufacturers using MDO frameworks and sophisticated CAD/CAE equipment. A great deal of computational analysis is required to obtain optimum configurations to satisfy many objectives and design constraints. Disciplines such as aerodynamics, propulsion, flight mechanics, structures, and aeroelasticity, among others, are frequently considered in the optimization framework to obtain more realistic geometries of flight vehicles and, recently, the addition of flight profile and mission analysis has been added [28]. Nowadays, many design variables (and types) may be employed, and advanced optimization algorithms that enable complex models of the aeronautical disciplines may be considered. Empirical formulae like the Class-I and -II methodologies proposed by Torenbeek [6] and Loftin [7] for drag and weight estimation are still used because they provide faster results [8].

Despite the rapid computer development and computational techniques, CFD analysis of complex aircraft configurations is still time-consuming, thus hampering in part its application in aircraft conceptual and preliminary design. Aerodynamic analysis requires considerable computational resources and labor work for the construction of complex 3D computational meshes, necessary to produce credible results. The case is even worse for multi-disciplinary optimizations, which deal with high-dimension problems that may reach thousands of design variables and their relationships. However, surrogate techniques have been increasingly adopted to model the physics with enough precision while at the same time reducing the computational time of complex and heavy calculations in MDO frameworks [28] [29].

The use of gradient-based optimization algorithms associated with adjoint methods is an alternative to considerably cut the processing time of optimization problems since their computational cost does not strongly scale up with the number of design variables compared to evolutionary algorithms [30]. There are two approaches for the adjoint method: continuous adjoint, by deriving the exact adjoint equation and then linearizing it; or the discrete adjoint, by directly deriving it from the discretized flow equations [30]. Both approaches compute the adjoint variables by an additional linear system of equations. Afterward, together with the mesh sensitivities, the final sensitivities, or gradients, are evaluated and transferred to an optimizer. On the other hand, there are some disadvantages to the adjoint methodology:

- Huge and long tasks must be carried out in preparation for several third-party codes to be used for automatic differentiation algorithms (Their source codes sometimes are not available).
- Usually, only mono-objective optimization for aircraft conceptual design is possible. For objectives encompassing several disciplines, the approach employed by adjoint optimization frameworks is to proceed with a weighted sum of objectives.
- It is challenging to consider optimization problems with discrete variables.
- It is characterized by low flexibility in changing constraints and objectives.
- Adjoint methods can handle tens of thousands of variables to define a wing geometry. However, airfoil geometry can be defined by ten or a few more variables by using parametrization like PARSEC [55].

Genetic algorithms, an evolutionary approach based on their metaheuristic of reproduction of the fittest, have widespread and effective use in the optimization of aircraft configuration [32] [33]. The procedure of reproduction of the fittest is repeated until some established criterium to close the process is reached. Evolutionary algorithms solve both constrained and unconstrained optimization problems whose great advantage lies in the absence of the necessity of gradient calculation of the objective function concerning the design variables. Opposed to this, is that this necessity is present in classic gradient optimization methods such as gradient descent and quasi-newton methods.

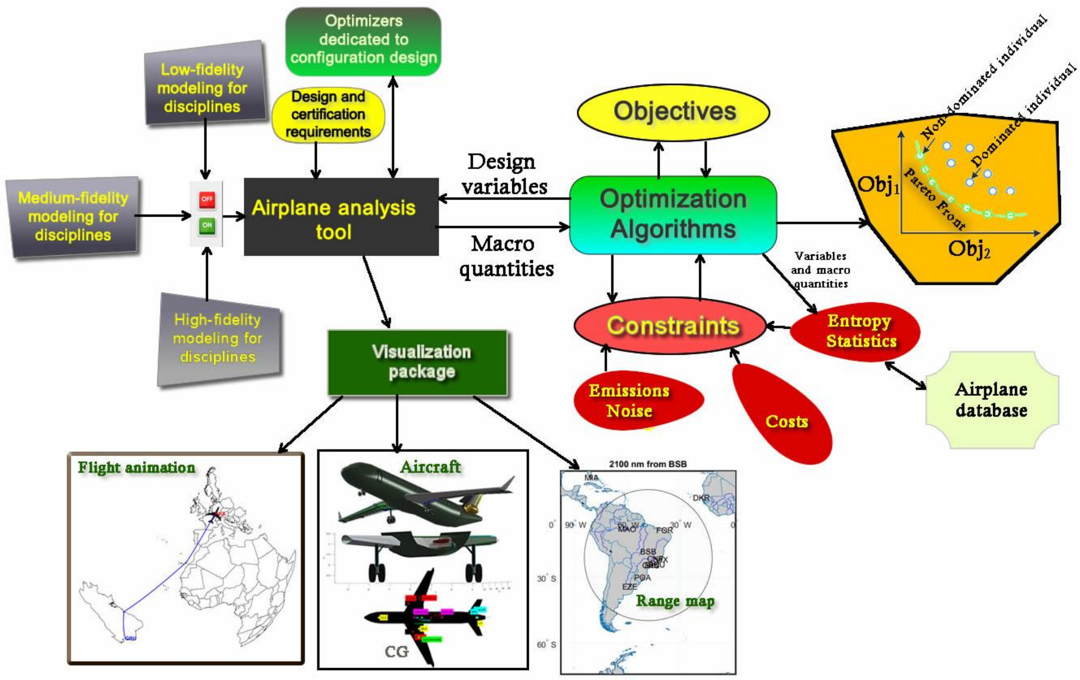

Figure 14: The MDO platform workflow of the present methodology

The workflow of the airplane design framework of the present work is shown in Figure 14. There are many possibilities in terms of fidelity of the discipline modeling that is used for airplane sizing. For example, lift-drag characteristics can be calculated by Class-I formulations as well as CFD codes, or even by surrogate ANN models [29]. In the present work, multi-objective genetic algorithms were chosen to perform the optimization runs.

Important design requirements must be considered because when satisfied, they will generate a feasible airplane configuration. Certification requirements such as climb gradient in 2nd segment, cruise and missed approach thrust requirements, rate of climb at service ceiling, and balanced takeoff field length are some of them.

The airplane classification provided by the entropy statistics approach was incorporated into the MDO platform. For the optimization runs carried out in the present work a category among the four shown in Figure 3 was set as a constraint. The service entry is a time variable used by the entropy statistics algorithm to perform the calculation of the convergence and diffusion indexes required for product classification. The year 2017 was selected as a reference year for all airplane configurations handled by the genetic algorithm to perform the classification procedure. The algorithm searches the airplanes in a database consisting of 123 jet airliners and selects configurations with service entry before and after the reference year within a prescribed timeframe (5 years in the present work).

Objectives

Objective 1: efficiency index

The authors elaborated a parameter that synthesizes the value of an airliner and that was designated here as the efficiency index:

$$EI_{Liner} = \frac{\widehat{Rnm} \times MMO \times \widehat{NPAX}}{\left(TW \times \widehat{OEW}\right)} \tag{5}$$

The symbols in **Eq. 4** are:

$$\widehat{NPAX} = \frac{NPAX}{150} \quad \widehat{Rnm} = \frac{Rnm}{2500} \quad \widehat{OEW} = \frac{OEW}{40000}$$

A low-efficiency index may be an indication of a low range, low cruise speed, or a high OEW for the mission it was conceived for. A low speed may appear not to be important, but it can be translated into a longer block time that impacts DOC. Besides, slower airplanes are obligated by air traffic control to fly at lower altitudes to avoid spoiling faster airplanes, causing in general higher fuel consumption. For business jet, which presents a different mission profile than that for airliners, the following efficiency index is proposed:

$$EI_{BJ} = \frac{\widehat{Rnm} \times MMO \times \widehat{CV}}{\left(TW \times \widehat{OEW}\right)} \tag{6}$$

In Eq. 5, $\widehat{CV}$ is the passenger cabin volume, given in m^3, divided by a normalization parameter. This figure excludes the baggage compartment. The value for the normalization of this parameter adopted here is 30 m^3. This parameter replaces the passenger capacity used in the composition of the EI_{Liner}.

The efficiency index for three ultra-long-range airplanes was calculated to verify if there is some degree of dependency of the index with the number the engines. The airplanes are the Boeing 747-400, the McDonnell Douglas DC-10-30, and the Boeing 777-200. Table 13 shows the results of the EI calculations and testifies that a three-engine configuration here presents a higher value than a two-engine airplane. An efficiency index comparison for some business jets was performed (Table 14).

Table 13: Efficiency index calculated for long-range airplanes with different motorizations

Airplane	n_e	MTOW [kg]	Single engine thrust [lb]	Two-class seating	Range$^\beta$ [nm]	EI
B747-400 [56]	4	362,874	57,000	358$^\alpha$	6,100	1.436
McDonnell Douglas DC-10-30 [57]	3	251,774	51,000	270	5,200	1.212
Boeing 757-200$^\gamma$ [58]	2	115,650	43,500	192	3,272	0.862
B777-200 [22]	2	229,500	71,200	375	3,750	1.050
Boeing 767-300 [59]	2	159,700	57,000	261	3,900	0.996
α The-class configuration: 24 first, 74 business, 302 in economy β Typical seating, MTOW, γ High-gross option						

Table 14: Efficiency index calculated for long-range airplanes with different motorizations

Airplane	n_e	MTOW [kg]	Single engine thrust [lb]	Range [nm]/pax	EI_{BJ}
Falcon 900 LX [60]	3	22,225	4,750	4000/8	6.99
G550 [61]	2	41,314	15,385	6750/8	6.10
Falcon 6X [62]	2	35,135	13,460	4900/8	4.26
Legacy 650E [63]	2	24,100	9,020	3800/8	4.85

Most airlines in current operation are fitted with turbofan engines due to some airline requirements. A third central engine like the one from McDonnell Douglas DC-10-30 is difficult to remove for overhaul. Besides, crews during pre-flight inspections must inspect the engines to assure that there are no problems like instance oil or fuel leaks and no visible debris. For an engine located in the vertical tail root, this presents a formidable task. However, another drawback of the trijet transport airplanes is that the wings must be located further aft on the fuselage due to the weight of the central engine that moves the center of gravity afterward. This, compared to twin jets and quad jets with all wing-mounted engines, will require vertical and horizontal tails of larger areas. On the other hand, a factor for sizing the vertical tail is the failure of an engine at takeoff. Considering that the thrust asymmetry of a trijet is lower than that of a twinjet, this will contribute to a smaller vertical tail.

Engines are priced according to the thrust they deliver established by contract clauses. If a trijet configuration could demand a lower overall thrust for a given set of requirements, this would contribute to lowering the manufacturing cost of such configurations. Besides, there is the important benefit of reduced emissions. However, the integration cost for assembling the central engine at the vertical tail root could nullify those benefits.

Unlike transport airplanes fitted with two engines, trijets are not required to land immediately at the nearest suitable airport if one engine fails. This is advantageous if the aircraft is not near one of the operator's maintenance bases, as the pilots may then proceed with the flight and land at an airport where there are more resources for maintenance. Additionally, trijets on the ground with one engine inoperative can be allowed to perform two-engine ferry flights. Before the introduction of ETOPS, only trijets and quad jets were able to perform long-range international flights over areas without any diversion airports. However, this advantage has largely disappeared since two-engine aircraft were certified for such operations.

Dassault claims that trijet design enhances comfort and performance and allows for a large cabin within a compact fuselage. The tri-engine airplanes present lower critical speeds for safer landings and superior short-field agility. Besides, the French manufacturer adds that trijets are more maneuverable on the tarmac, require less hangar space – and provide greater peace of mind and more direct routing on long routes over water.

Objective 2: direct operating cost

Although it is widely discussed which cost elements do belong to *Direct* Operating Costs and which do not, it is generally accepted that DOC includes those cost elements which depend on the equipment (aircraft) and crew that are necessary to perform a determined flight. *Indirect* Operating Costs (IOC), in contrast, are dependent on the way an airline is administrated [64]. The ATA 67 DOC method [65], a good reference, considers aircraft-dependent and hence part of DOC:

- cockpit crew costs,
- fuel costs,
- maintenance costs,
- depreciation,
- insurance (against hull loss).

Cockpit crew cost is heavily dependent on MTOW, and it is calculated in terms of flight hours. Training costs for the crew or maintenance personnel traditionally are considered as a percentage of the crew's fixed cost. For the engine, it is necessary to provide to the DOC calculation routine the number of engines, the engine weight, and the time between overhauls that are considered.

Figure 15 displays the result of a direct operating cost estimation performed for the hypothetical 76-seat ITA76ADV airliner with a design range of 2100 nm. The calculation considered two jet-fuel prices, US$ 1.70 and US$ 2.389, a 40.6% increase. The contribution to DOC increased from 25% to 31%, surpassing the crew slice related to that cost. Thus, as expected, the DOC is indeed sensitive to fuel price.

The values here calculated for the DOC have estimated values and no comparison to actual values practiced by airlines is possible, because they handle this information as strategical and confidential. Nevertheless, it offers a relatively good basis for comparison among the airplanes that are an object of investigation. It is worth mentioning, that changing the fuel price will, as shown in Figure 15, significantly alter the way the airplanes are evaluated, and eventually it could be part of a Pareto front. Ref. [66] provides graph information about the annual variation in jet fuel price.

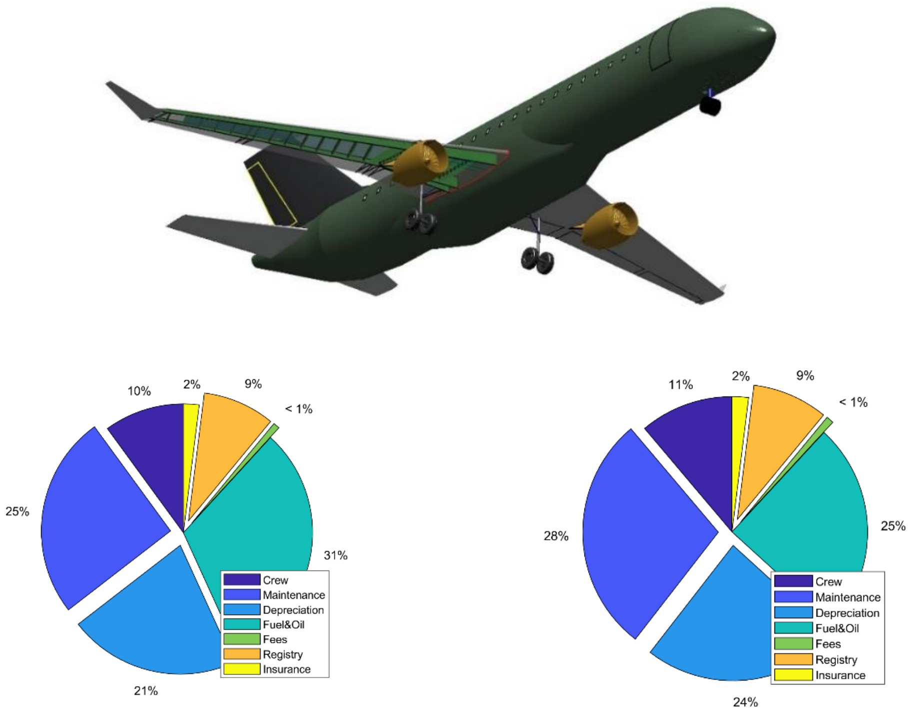

DOC: US$ 10.82/nm
Jet A1: US$ 2.387/gallon

DOC: US$7.85/nm
Jet A1: US$ 1.70/gallon

Figure 15: DOC breakdown for the ITA76ADV considering two Jet A1 fuel prices

Optimization tasks

Optimization algorithms are employed for the following tasks:

- To find the weights for airfoil geometries, so that they can be described by an airfoil database. The purpose of this task lies in providing wing geometry input for aerodynamic coefficient calculation by a neural network.
- To obtain the intersection surface between a high wing configuration and the fuselage.
- For optimization of the wing structural layout.
- For sizing of the vertical tail.

  For wing airfoil optimization when required by the user.

For all multidisciplinary optimization runs of the present work two objectives were set and will be detailed later. The optimizations can be categorized into two profiles:

Type I. Here, the maximum takeoff thrust is one of 13 design variables. Engine diameter and overall pressure ratio are fixed parameters provided to the airplane calculator program. The variation of thrust and altitude were modeled according to Howe's approach [67]. Four runs were performed. Each one of them had a different classification constraint for the airplane configuration: classic, breakthrough, failure, and niche.

Type II. This is an improvement for airplane modeling when compared to the previous simulations. An engine deck was introduced as part of the aircraft analysis tool package. There are five definition variables plus some additional parameters for engine characterization. Thus, the engine is designed jointly with the airframe. A total of 17 design variables are considered in this simulation.

The boundaries of the variables for the Type I optimization problems are shown in Table 15**.** The second optimization type utilizes another approach for engine modeling, and it is an improvement for airplane representation when compared to the simple engine model used in the previous type. It is important to emphasize the fact that, all engines in Type I simulations made use of a hypothetical turbofan whose reference TSFC at cruise is 0.55 lb/h/lb. Now, a generic turbofan engine deck was introduced as part of the aircraft analysis tool package to improve aircraft modeling. Its theoretical approach and validation are given in Ref. [40]. A map for compressor efficiency calculation and other improvements and features were added such as engine noise and emission estimation [10]. The present modeling does not contemplate new engine concepts like geared turbofans. There are five variables for the engine and additional parameters for engine characterization, such as the Mach number and altitude of the design point. Thus, the engine is designed jointly with the airframe. A total of 17 design variables were considered in this simulation. The variables and their boundaries of the present optimization problem are depicted in Table 16

Table 15: Boundaries of variables of the optimization problem considering overall maximum thrust as a design variable

Variable	Lower boundary	Upper boundary
Wing reference area [m^2]	120	300
Wing aspect ratio	8.0	10.9
Wing taper ratio	0.240	0.450
Wing quarter-chord sweepback angle	22°	32°
Fuselage length [m]	36	60
Number of seating rows	6	7
Range with typical passenger payload (ISA, no winds)	2100	3700
Height/width of central fuselage [m]	0.90	1.10
Number of engines$^{\alpha}$	2	3
MMO	0.78	0.83
Overall engine thrust @ takeoff [kN]	220	500
Service ceiling [ft]	35,000	42,000
Number of corridors in the passenger cabin	1	2
α the trijet configurations have two underwing engines and a third one located on the vertical tail root		

Table 16: Boundaries of variables for Type II optimization problem

Variable	Lower boundary	Upper boundary
Wing reference area [m^2]	120	300
Wing aspect ratio	8.	10.9
Wing taper ratio	0.240	0.450
Wing quarter-chord sweepback angle	22º	32º
Two-class passenger accommodation	150	280
Number of seating rows	6	7
Range with typical passenger payload (ISA, no winds)	2300	4000
Height/width of central fuselage [m]	0.90	1.10
Number of engines	2	2
Service ceiling [ft]	35,000	42,000
Number of corridors in the passenger cabin	1	2
Engine by-pass ratio	4.4	6.2
Engine diameter [m]	1.50	2.80
OPR	26:1	33:1
FPR	1.20	1.83
Turbine inlet temperature [K]	1250	1455

Some aircraft parameters that were set for all simulations simulation are:

- Year of service entry: 2017.
- Engine TBO of 3000 h.
- Container to be accommodated in cargo compartment: LD3-45W.
- The relative maximum thickness of root airfoil: 15.5%.
- The relative maximum thickness of root airfoil: 11.0%.
- Passenger cabin height of 2 m.
- Y-class seat width of 0.46 m.
- Y-class seat pitch of 0.8128 m.
- Business-class seat pitch of 0.9144 m.
- Aisle width of 0.48 m.
- Vertical tail volume coefficient of 0.09.
- Horizontal tail volume coefficient of 1.
- Fuselage tank in front of the wing leading-edge extension.
- Takeoff field length lower than 2400 m (MTOW, ISA, sea level).
- Must comply with FAR requirements for 2nd segment climb.
- Must comply with FAR121 requirements for balked landing.
- Must comply with FAR119 requirements.
- Enough thrust to cruise at the prescribed altitude.
- Jet A1 fuel price US$ 2.387 US$/gal.
- Location of the aft wing spar at 72% of chord.
- Takeoff flap deflection of 25º.
- Landing flap deflection of 40º.
- Long-range cruise profile.
- No emissions or noise constraints.

3. Entropy-statistics classification as a constraint in an optimization problem

Type I and II optimization runs were carried out here. For Type II, the classification constraint classic was the only one used just to compare its results with the related Type I simulation.

The Type I simulation additional parameters are:

- Three types of product classification: classic, niche, and failure.
- Engine by-pass ratio of 6.
- Engine external diameter of 1.715 m.
- Engine overall pressure ratio of 32.2.
- TSFC at long-range cruise of 0.55 lb/h/lb.

Although attempted, no feasible configuration emerged from the Type I simulation with the airplane classification set as a breakthrough. As already explained in the preceding paragraphs, this result is due to the year of service entry chosen for the present simulations, namely 2017, the airplanes present in the database, and the limitations of the aircraft modeling employed here.

No engine deck was employed in the simulations where the overall thrust was provided. The engine parameters here were used to estimate the engine length, and therefore the engine weight, which is necessary for the DOC calculation, and the wetted area, which is important for drag calculation.

3.1 Multi-objective optimization with overall thrust as a design variable

Classic designs

A multi-objective optimization design run was carried out where the constraint for airplane classification by entropy statistics was set as classic. After 50 generations with the MATLAB® multi-objective genetic algorithm, the number of feasible individuals is 1980 – which is the number that does not violate any constraint (Figure 16). Some configurations with two aisles and presenting six or seven seating rows emerged in the computation and were categorized as classic but none with seven rows or two corridors are part of the Pareto front. In addition, all feasible airplanes that emerged from the simulation are fitted with two engines. The configurations with two aisles are the heaviest and are expected to present a higher DOC. The main advantage of this configuration is to propitiate more comfort to the passenger. However, the present simulation also allows for more fuel capacity of the tank located in the fuselage.

This is mainly due to the engine characteristics that were chosen for the optimization tasks. Those characteristics are closer to modern and fuel-efficient engines in the category of the A320 and B737 airplanes. The engine that was then selected, presents a fuel consumption at long-range cruise conditions approximately 8% lower than the one of IAE V2500-A5. The departure of the A320 basic design was minimal among the airplanes with the same range and capacity as of A320-200.

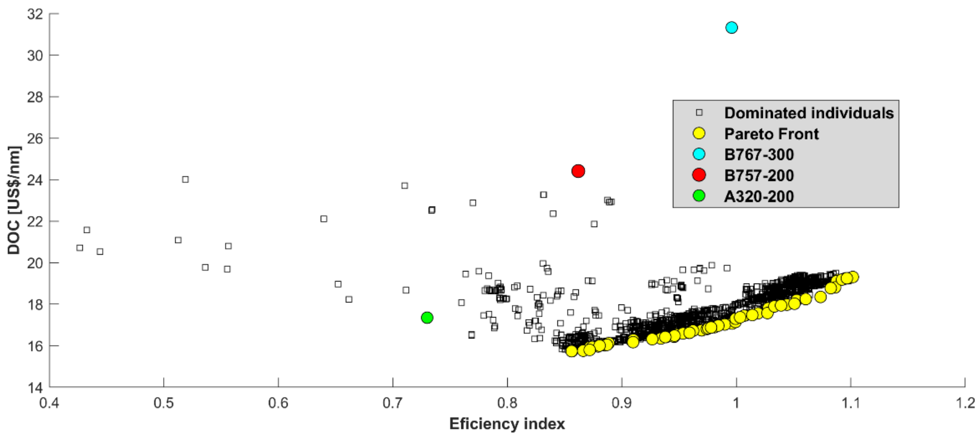

Figure 16: Pareto front for classic designs. Calculated values by the present design framework for B757 and A320 are plotted for comparison purposes, only

As was performed for A320-200, the efficiency index and DOC values for B757-200 are displayed in Figure 16 for comparison purposes, only. Table 17 contains some featured individuals from the Pareto front, characterized for EI varying from 0.856 to 1.102. For the same efficiency index, the B757-200 airliner has a DOC US$ 5.1/nm higher than the one from ID 1845C, featuring the highest DOC from the configuration shown in Table 17.

Figure 17 shows some fuselage cross-sections from the individuals presenting the lowest and the highest DOCs and now a significant difference between them becomes evident. Figure 18 shows the top view for two individuals from the Pareto front featuring the lowest and highest DOCs. The geometric characteristics of ID 1031C are remarkably like those from A320-200 but with the exception that they present a design range of 3,005 nm which is considerably higher.

Table 17: Some individuals belonging to the Pareto front of the classic aircraft optimization

ID	MTOW [kg]	OEW [kg]	Design range [nm]	Total thrust [kN]	NPAX	Aisle	Seating rows	DOC	EI
1031C	74,000	42,092	3,005	225	140	1	6	15.74	0.856
1963C	73,975	41,666	3,006	225	140	1	6	15.80	0.872
1138C	82,222	45,843	3,124	242	162	1	6	16.97	0.984
1704C	85,997	47,983	3,177	245	172	1	6	17.56	1.019
1868C	90,380	50,153	3,274	263	180	1	6	18.19	1.053
1738C	95,759	52,637	3,392	279	192	1	6	19.17	1.089
1845C	96,576	52,867	3,415	281	192	1	6	19.31	1.102

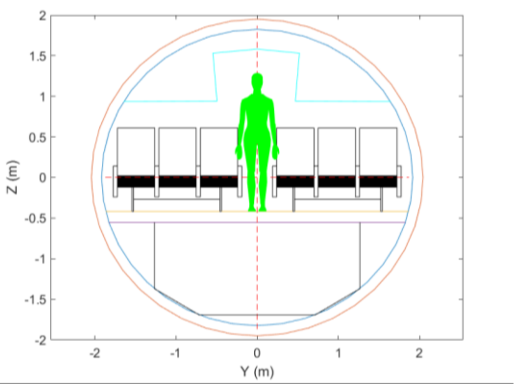

ID 1031C

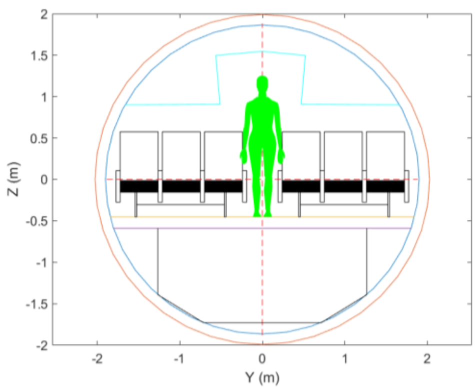

ID 1845C

Figure 17: Cross-sections of some individuals in the Pareto front from the optimization run for classic airplanes

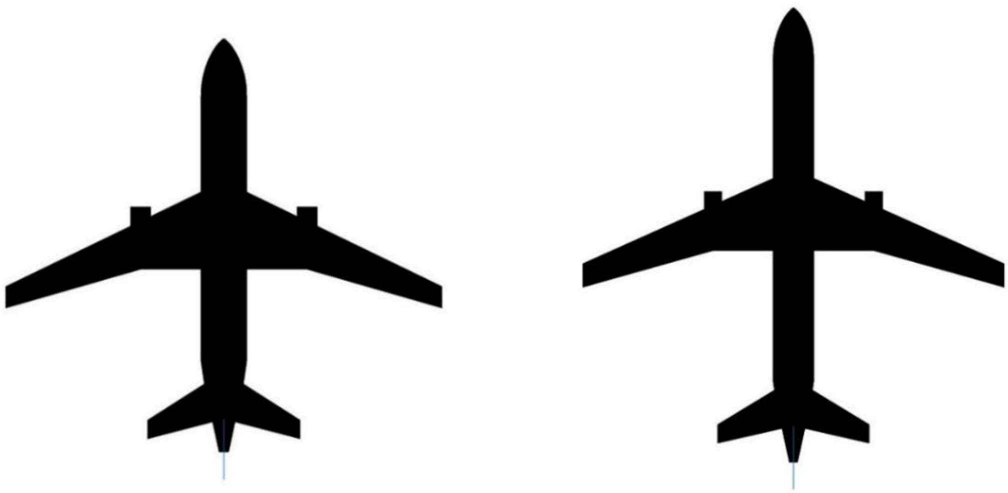

ID 1031C ID 1845C

Figure 18: Top view of some individuals in the Pareto front of classic design simulation (not on the same scale)

Figure 19 shows the DOC divided by passenger accommodation for all individuals from the simulation. There is an almost linear relationship between the efficiency and the DOC per passenger. All individuals in the Pareto front present the DOC per passenger lower than that registered by the B757-200.

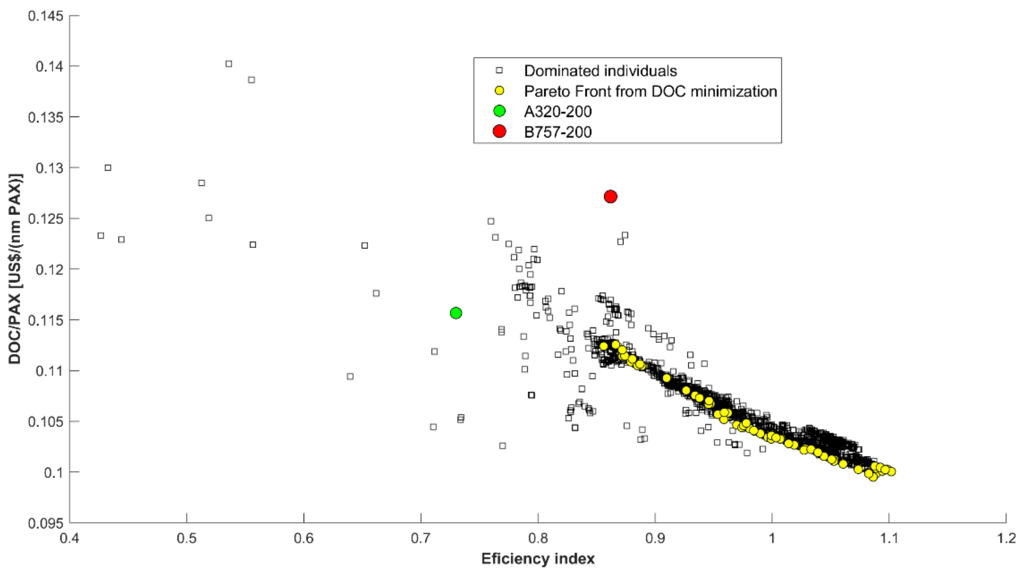

Figure 19: DOC per passenger two-class capacity plotted against efficiency index for all feasible airplanes from the optimization run

To verify which individuals from the Pareto front are closer to B757-200, a Dendrogram approach was elaborated. This time the variables used to build up the distance matrix are related to configuration geometric characteristics and performance parameters, but not to weights and engines. The reason for this is because the point of interest is to find out an airplane with higher efficiency index and lower DOC that is related to a configuration with lower MTOW and OEW.

The variables that were used to compose the dendrogram are the following:

- Wing area
- Wing aspect ratio
- Wing quarter-chord sweepback angle
- L_f
- Design range
- Fuselage height-to-width ratio
- MMO
- TW
- Wing taper ratio
- Service ceiling
- Two-class passenger accommodation
- Number of aisles
- Engine configuration
- Seating rows in Y-class

Figure 20 shows the resulting Dendrogram for the four closest individuals to the B757-200 configuration.

Table 18 contains a comparison among some characteristics of the closest individuals to B757-200. The configuration of ID 1785C (Figure 21) was found to be the most resemblance to the B757-200. It surpasses the veteran airliner in all aspects: lower DOC, 20 t lower MTOW, and considerably lower OEW for the same passenger capacity and almost the same range. MMO of 0.82 is lower than that of B757-200.

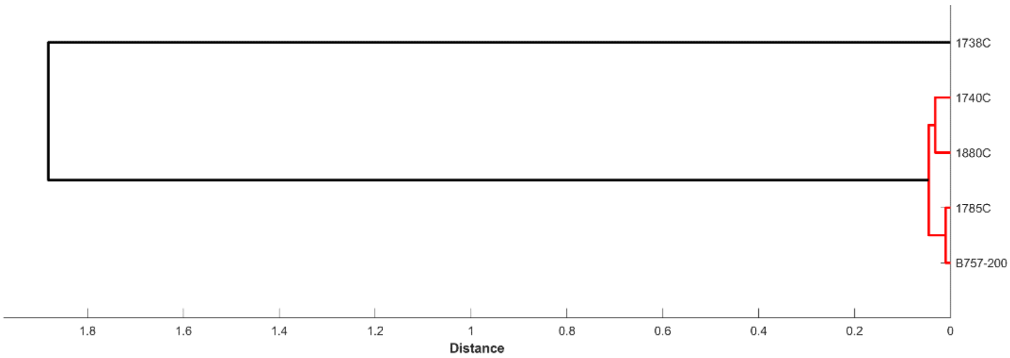

Figure 20: Dendrogram of the closest configurations to B757-200

Table 18: Closest individuals to B757-200

ID	wS [m²]	wAR	MTOW [kg]	OEW [kg]	Design range [nm]	Thrust [kN]	NPAX	DOC [US$/nm]	EI
1740C	167.4	10.5 3	96,067	52,754	3,397	279	192	19.22	1.094
1880C	168.6	10.3 2	95,743	52,486	3,399	279	192	19.19	1.092
1785C	167.4	10.3 5	95,253	52,276	3,387	277	190	19.11	1.088
B757-200	**185.25**	**7.8**	**115,650**	**58,570**	**3,476**	**351**	**192**	**24.41**	**1.014**

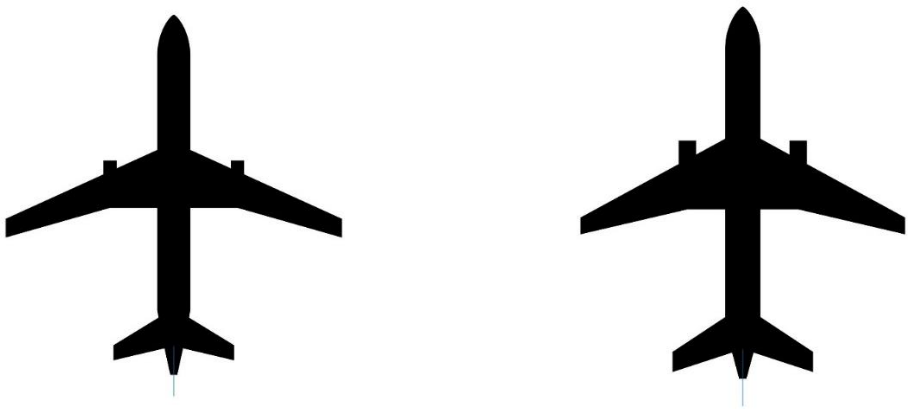

ID 1785C B757-200

Figure 21: Top view of B757-200 and its closest potential replacement that emerged from optimization run for classic airliners (not on the same scale).

Niche designs

The optimization run with a constraint stipulating that the airplanes must obey the classification as the niche was carried out and was stopped after 25 generations. Each generation was populated with 55 individuals. Just 693 individuals were revealed to be feasible, and 40 of them are part of the resulting Pareto front. Some characteristics of airplanes found in the Pareto front are:

- All are fitted with 3 engines.
- All feature 2 aisles and a T-tail.
- Two-class passenger capacity in the 177-236 range.
- DOC is equal to or higher than 17.88 US$/nm.

Figure 22 shows the objective values of the feasible individuals from the optimization run for niche airplanes. The niche airplanes belong to the Pareto front individuals from the optimization with the classification constraint *niche*. Table 19 contains characteristics of some individuals from the Pareto front sorted by ascending DOC. Considerably higher EI was found than those that emerged from the classic airplane simulation.

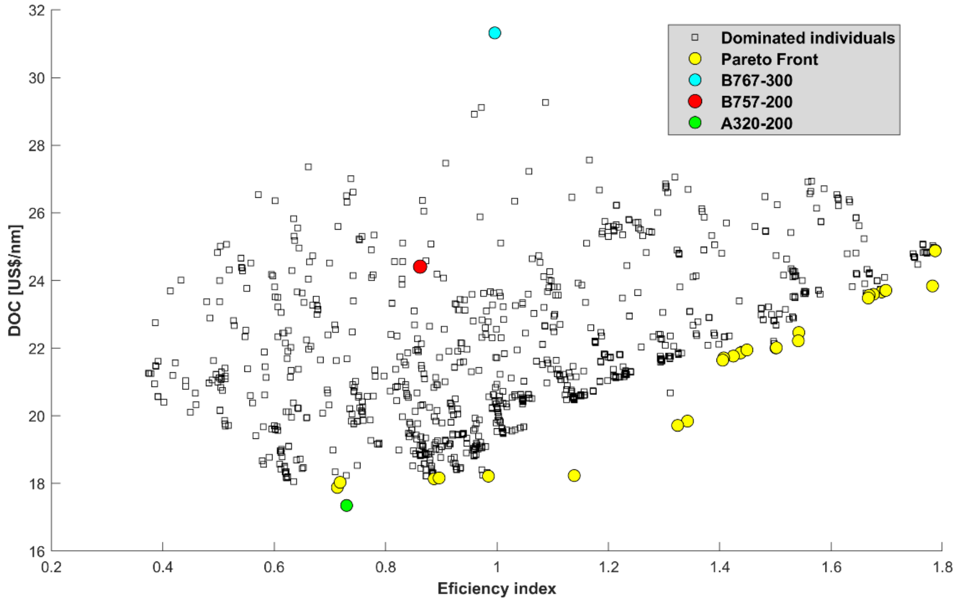

Figure 22: Optimization considering niche airplanes

Table 19: Individuals belonging to Pareto front of optimization for niche aircraft

ID	MTOW [kg]	OEW [kg]	Range [nm]	T [kN]	NPAX	Rows	DOC [US$/nm]	EI
1393N	81,676	48,715	2,708	238	150	6	17.88	0.713
1025N	89,217	49,269	3,632	286	148	6	18.14	0.887
1356N	90,155	49,269	3,632	286	150	6	18.16	0.896
1321N	116,630	63,679	3897	286	216	6	21.65	1.405
986N	116,450	62,165	3,897	286	216	6	21.86	1.437
1132N	129,020	63,045	3,897	286	228	6	22.46	1.542
1074N	129,540	68,579	3,897	286	252	7	23.71	1.698
1332N	138,400	74,557	3,897	286	273	7	24.89	1.787
Boeing 757-200 [27]	**115,650**	**58,570**	**3,272**	**387**	**192**	**6**		
Boeing 767-200 [59]	**136,078**	**80,286**	**2,750**	**454**	**216**	**7**		

Figure 23 shows the DOC divided by passenger accommodation for all individuals from the simulation. Contrary to the previous simulation, there is not a direct relationship between the efficiency index and the DOC per passenger. All individuals in the Pareto front present the DOC per passenger lower than the one registered by the B757-200. However, the individuals from the Pareto front with EI higher than 1.4 present better figures and should be chosen for further analysis by a decision-making team.

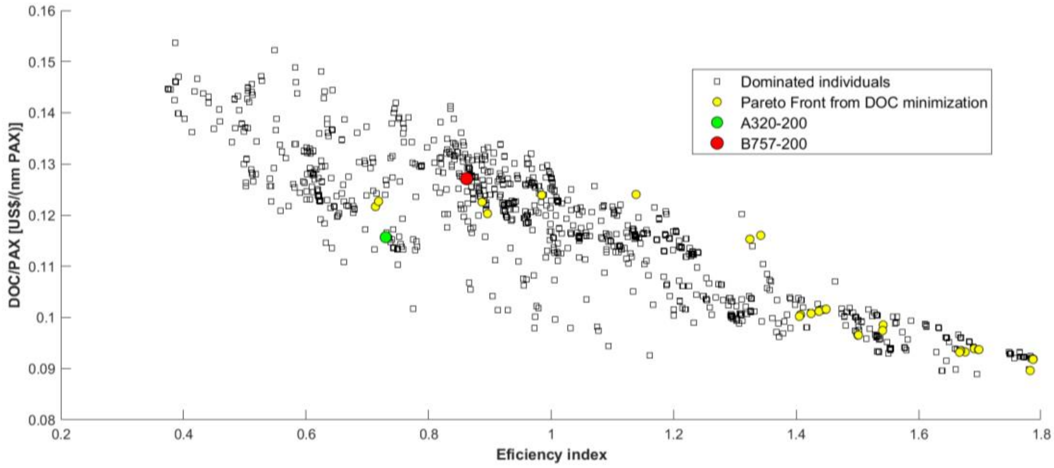

Figure 23: DOC per passenger two-class capacity plotted against efficiency index for all feasible airplanes from the optimization run with niche constraint

In terms of capacity, the ID 1321N configuration is the one closer to B757-200 with the lowest DOC. The range with 216 passengers is 3,897 nm and for the reference capacity of 192 passengers, it will fly farther than 4,000 nm. Its maximum engine thrust is also considerably lower than that of B757-200 fitted with RB2111-535E4 engines (Table 11), but the wing reference area is higher, 228.41 m^2. Cross-sections of three individuals from the Pareto front are compared in Figure 24 and Figure 25 displays their top views. It is important to stress that airplane classification by entropy statistics depends on the year of the aircraft's entry into service. Considering the airplanes present in the database, there are no three-engine aircraft in the timeframe of 5 years around 2017. For this reason, airplanes with this configuration will be considered anything other than classic. No breakthrough design emerged from the optimization simulation with this constraint. Thus, there are only three simulations with optimal configurations: classic, niche, and failure.

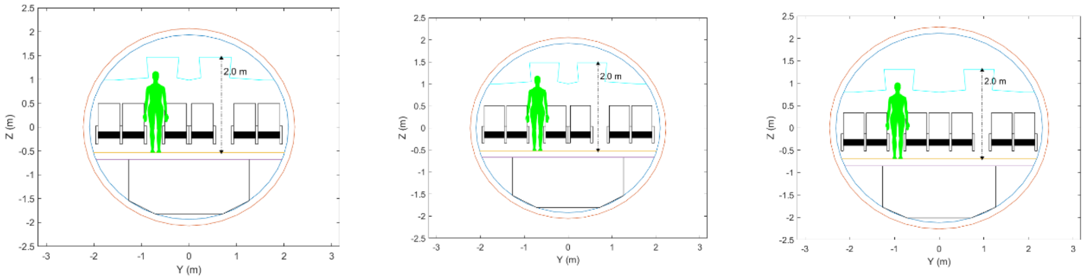

ID 1393N ID 986N ID 1332N

Figure 24 – Cross-sections of some individuals in the Pareto front from the optimization run for niche airplanes

ID 1393N ID 986N ID 1332N

Figure 25: Top view of some individuals in the Pareto front of niche design simulation (not on the same scale)

Failure aircraft

All failure designs that emerged in the simulation in the Pareto front (Figure 26) share the following characteristics:

- Six rows of seats
- Single aisle.
- Three engines and a T-tail.

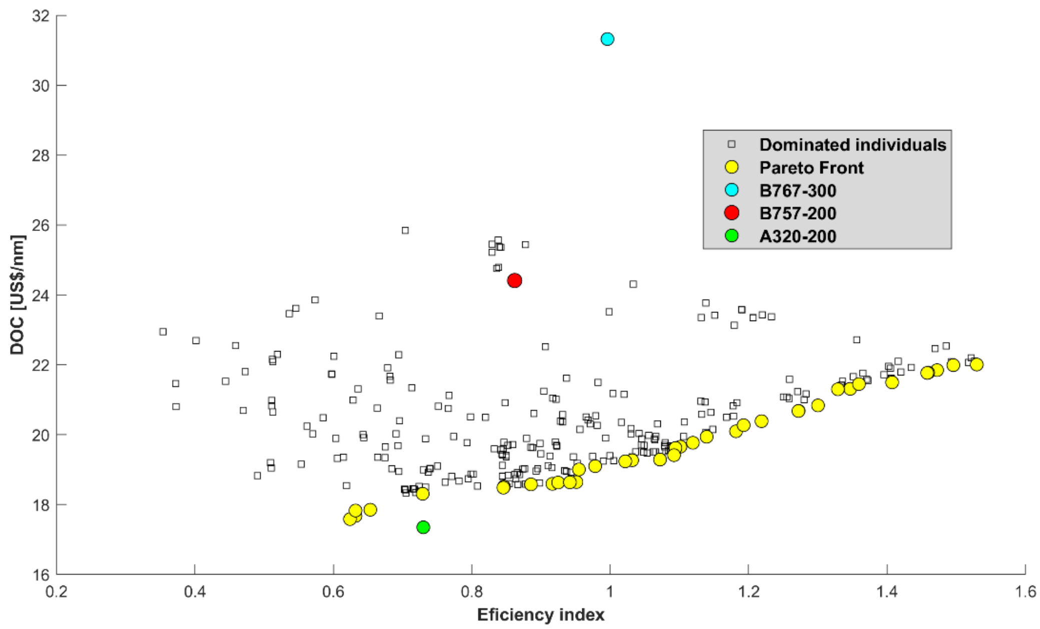

Figure 26: Optimization considering failure airplanes

For the same EI, Airbus A320-200 presents a DOC lower than its counterpart in the Pareto front. Table 20 contains some characteristics of selected individuals from the Pareto front. There are airplanes in the 148-234 range. The airplane with the same capacity as the B757-200 reference aircraft, carrying the ID 241F, presents higher efficiency and lower DOC in comparison. The top view of some optimal configurations is shown in Figure 27.

Table 20 – Individuals belonging to Pareto front of optimization for failure aircraft

ID	n_e	MTOW [kg]	OEW [kg]	Range [nm]	T [kN]	NPAX	Aisle	Rows	DOC [US$/nm]	EI
320F	3	78,552	45,879	2,817	286	144	1	6	17.59	0.624
290F	3	90,944	50,070	3,473	289	168	1	6	18.64	0.42
163F	3	91,703	49,928	3,713	262	162	1	6	18.65	0.951
200F	3	97,035	52,718	3,714	293	180	1	6	19.29	1.072
241F	3	100,000	53,201	3,714	294	192	1	6	19.94	1.139
362F	3	116,900	63,593	3,713	262	234	1	6	22.01	1.530

Figure 27: Top view of some individuals in the Pareto front of failure design simulation (not on the same scale)

3.2 Optimization of airframe engine design concomitantly

The Pareto front is shown in Figure 28, with the EI and DOC of reference airplanes for comparison purposes. Table 21 contains the characteristics of some relevant individuals in the Pareto front. Further selections of individuals of Pareto front that present passenger capacity like the one of Boeing 757-200 is given in Table 22. All of them are fitted with engines featuring by-pass ratios of 6:1, presenting ranges slightly longer than the Boeing-757-200, with considerably lower MTOW, as well as lower engine maximum thrust. Figure 29 displays some top views of three configurations from the Pareto front.

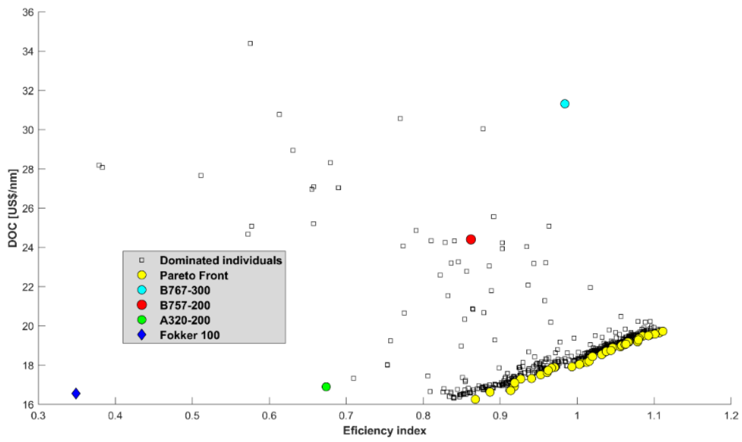

Figure 28: Optimization run considering a turbofan engine generic deck

Table 21: Individuals belonging to Pareto front of optimization (Engine deck)

ID	n_e	MTOW [kg]	OEW [kg]	Range [nm]	T [kN]	NPAX	Aisle	Rows	DOC [US$/nm]	EI
470CE	2	75,872	43,119	3,027	215.74	142	1	6	16.26	0.868
727CE	2	79,055	44,514	3,090	225.93	150	1	6	16.70	0.914
662CE	2	86,236	47,504	3,171	247.40	168	1	6	17.92	0.993
755CE	2	90,113	49,332	3,282	261.41	174	1	6	18.44	1.020
744CE	2	93,752	50,838	3,360	271.33	180	1	6	19.05	1.063
725CE	2	96,040	51,836	3,403	278.95	186	1	6	19.37	1.080
435CE	2	98,125	52,729	3,421	285.67	192	1	6	19.66	1.107
731CE	2	98,600	52,934	3,431	287.22	192	1	6	19.73	1.112

Table 22: Optimal designs with passenger capacity and range similar to B757-200

ID	wS [m^2]	wAR	wTR	MTOW [kg]	OEW [kg]	Design range [nm]	Thrust [kN]	NPAX	DOC [US$/nm]	EI
731CE	176.4	9.94	0.295	98,600	52,934	3,431	287.2	192	19.73	1.112
726CE	170.85	10.08	0.309	95,657	51,799	3.351	275.9	186	19.29	1.080
303CE	175.5	9.97	0.296	98,124	52,729	3,420	285.6	192	19.67	1.107
B757-200	**185.25**	**7.8**	**0.243**	**115,650**	**58,570**	**3,476**	**387**	**192**	**24.41**	**1.014**

ID	wSw14	OPR	BPR	Engine Diameter [m]
731CE	22.26	32.18:1	6.02:1	1.93
726CE	23.14	32.42:1	5.96:1	1.89
303CE	22.29	32.21:1	6.00:1	1.93
B757-200	**25.0**	**25:1**	**4.40:1**	**2.20**

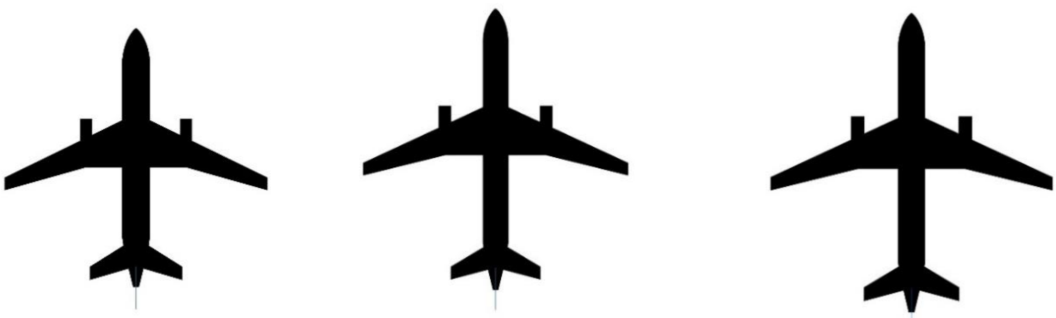

ID 470CE ID 303CE ID 435CE

Figure 29: Top view of some individuals in the Pareto front of classic design simulation (not on the same scale)

3.3 Featured choices

The main difference between classic and failure configurations concerns their number of engines, both present configurations with 6 seating rows. The niche and failure designs share the same number of engines, which is three. The characteristic that distinguishes the two groups is the number of corridors: two for the niche airplanes; one for those considered a failure. The Airbus A350 is present in the airplane database in the timeframe considered and this airplane has two corridors in its cabin layout. This characteristic was transmitted to some aircraft, and they could then be classified as niche. No airplane in the database, in the timeframe around 2017 that was set for the optimization runs, has three engines combined with a single corridor and this was enough to characterize the failure airplanes.

Figure 30 on the left contains all Pareto fronts of the four optimization runs. The Pareto front of the failure aircraft does not intercept any of the classic ones, intercepting the niche aircraft at approximately an EI of 1.42. The two optimizations for the classic airplanes are remarkably close to one another. The result observed here is that the niche configuration 1332N has the best efficiency index among the individuals of the three Pareto fronts. Due to this and its reasonable DOC for its category, it deserves a deeper analysis. This airplane is fitted with three engines. It was classified as a niche because there were no tri-engine airplanes before and after it, considering the timeframe of 5 years utilized by the classifier algorithm. The DOC takes into consideration the number of engines and their thrust. The 2nd segment climb requirement is very stringent for two-engine airplanes. Thus, depending on aerodynamics and weight, a three-engine airplane may present a lower thrust-to-weight ratio. The tradeoff between *TW* and the number of engines seems to be more favorable to configurations with three engines in some cases.

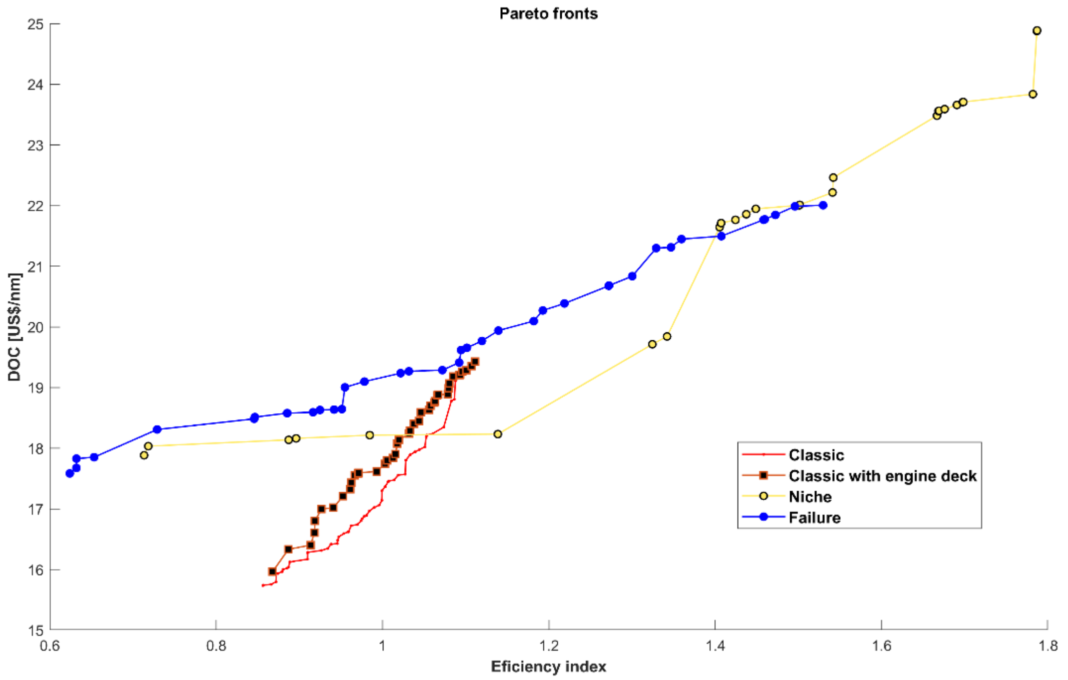

Figure 30: Plot combining all Pareto fronts from the present simulations

According to the simulation results, there are two choices for the possible fulfillment of MMA:

- Classic design: the ID 303CE is an extraordinarily strong candidate due to its considerably lower MTOW, OEW, and lower maximum takeoff thrust when compared to the B757-200 reference airplane. Its configuration is like the one of ID1845C.
- Niche design: 1332N is also a strong candidate due to its impressive efficiency index enabling a great range and passenger capacity. It will fulfill another part of the market for MMA. Niche candidates with EI above 1.4 present a better Doc per passenger (**Fig. 25**).

4. Robust optimization of a chosen individual of a previous optimization

This optimization task considers the fuel price ranging from 0.887 to 4.387 US$/nm and its impact on DOC for a mission of 3420 nm with 192 pax. The objectives are just the average DOC and its standard deviation. The intent is to evaluate whether an airplane configuration resilient to fuel price variation can be derived. An improved ANN system based on full potential formulation with viscous correction was employed in this simulation [68]. This time, the root, and the break station airfoils are part of the design effort. Table 23 presents the design variables and their boundaries for the present design task.

Table 23: Design variables and their boundaries

Variable	Lower boundary	Upper boundary
Wing reference area [m^2]	165	195
Wing aspect ratio	9	9.90
Wing taper ratio	0.240	0.380
Wing quarter-chord sweepback angle	22º	28º
Engine diameter [m]	1.62	2.20
Engine by-pass ratio	5.0	6.2
OPR	25:1	33:1
FPR	1.25	1.80
Turbine inlet temperature [K]	1250	1455
Root airfoil weights (14 in total)	0	1
Break station airfoil weights (14 in total)	0	1

By a slight reduction of the wing aspect ratio of the Design ID 303CE (Table 22), keeping the remained parameters but the root airfoil section of the wing unchanged, a baseline airplane was created for this last optimization task (Table 24). Mattos et al. [69] applied a flutter speed constraint to an MDO framework for airliner conceptual design. As optimization results, a noticeable reduction of wing aspect ratio was observed when compared with an optimization where no flutter speed constraint was applied.

Table 24: Baseline airplane for the robust optimization

MTOW [kg]	99277
OEW [kg]	53282
Fuel capacity [kg]	31121
wS [m^2]	175.45
wAR	9.90
wSw14	22.29º
BPR	6.00
OPR	32.21
Avg DOC [US$/nm]	20.960
Range with 192 pax at FL390 [nm]	3,420
DOC Standard deviation [US$/nm]	2.9986

The optimization task was stopped after 35 generations and slightly over 1300 feasible configurations emerged from the simulation. Figure 31 shows the relationship between MTOW and DOC for all feasible individuals. A linear correlation between the two variables can easily be recognized. Figure 32 shows the objective diagram containing optimal airplanes, feasible individuals, the baseline airplane, and the figures obtained in the present work for the B757-200 airliner. There are two individuals in the Pareto front with similar characteristics. This means a high degree of dependence on the two objectives chosen for this optimization task. Table 25 contains major information regarding one of the optimal airplanes. Its MTOW is 1,760 kg lower than that of the baseline airplane. This represents slightly over 18 t less than the Boeing 757-200 MTOW. All this was achieved thanks to the airfoil design and an engine featuring a higher by-pass ratio, with no "advanced" technology being incorporated into the configuration.

Regarding the baseline aircraft, the average DOC was decreased by 0.473 US$/nm. For a fleet comprised of 10 airplanes performing two flights a day operating 300 days/year, this will represent a cost saving of US$ 9.7 million. A direct comparison between the optimal and reference airfoil for the tip station is shown in Figure 33. Figure 34 shows the probability density function that resulted from all feasible airplanes analyzed in the robust optimization simulation.

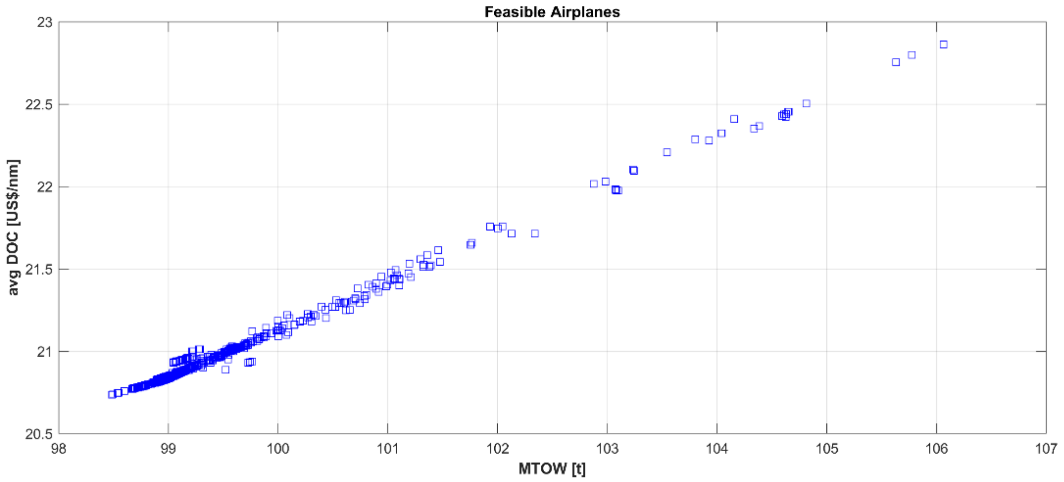

Figure 31: Linear dependence between DOC and MTOW

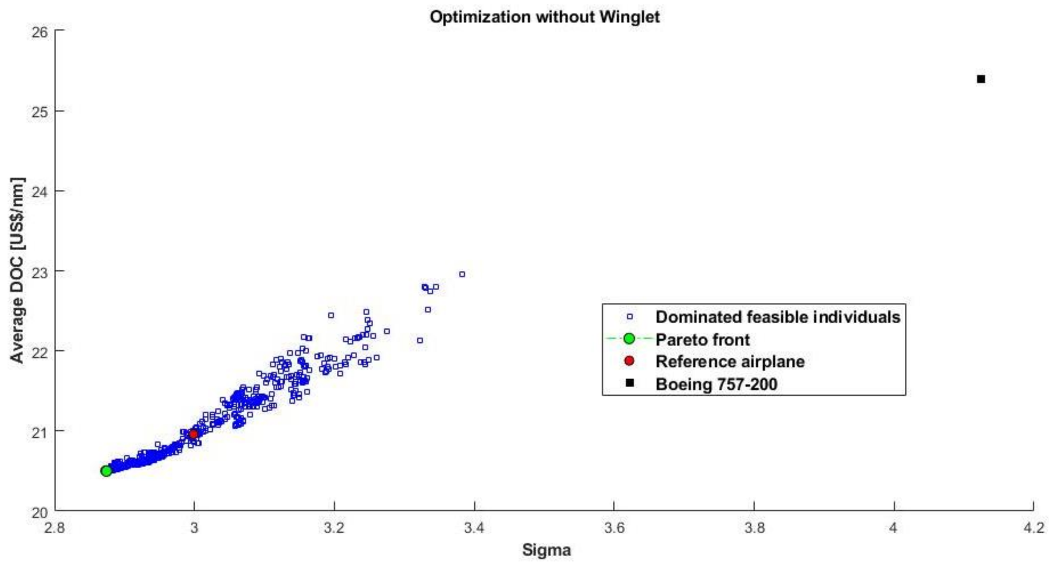

Figure 32: Objectives and feasible individuals

Table 25: Optimal airplane characteristics

MTOW [kg]	97517
OEW [kg]	52637
Fuel capacity [kg]	32118
wS [m^2]	175.51
wAR	9.886
wSw14	22.04º
Engine diameter [m]	1.925
BPR	6.19
OPR	32.60
Avg DOC [US$/nm]	20.487
DOC Standard deviation [US$/nm]	2.8724

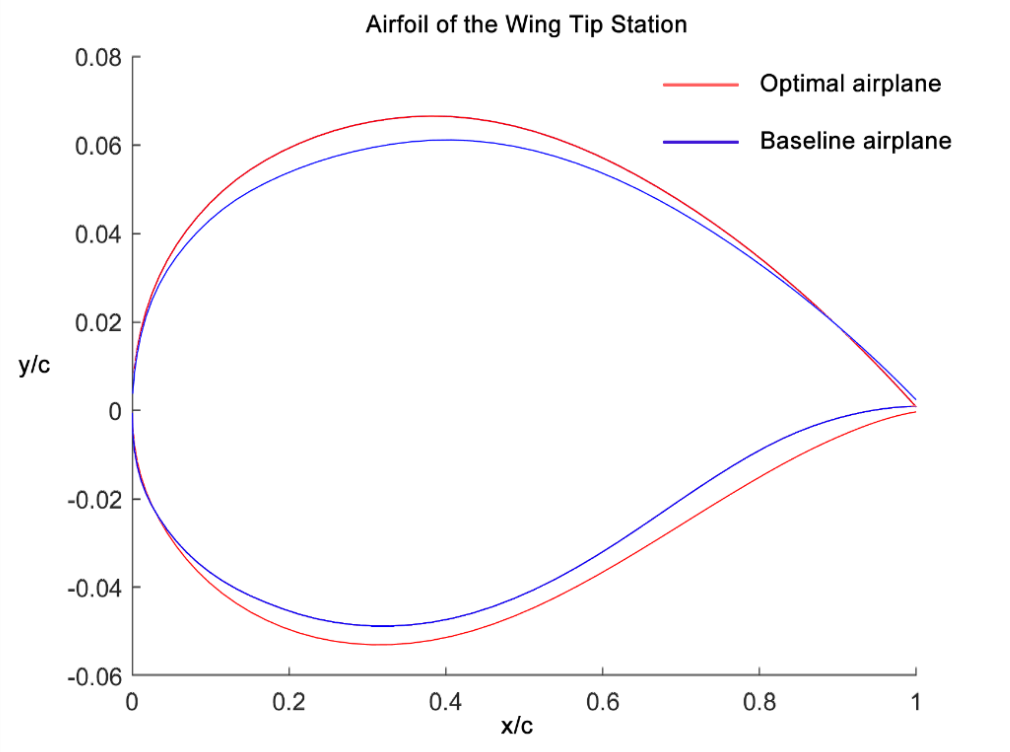

Figure 33: Comparison between optimal and reference airfoil of the wing tip station

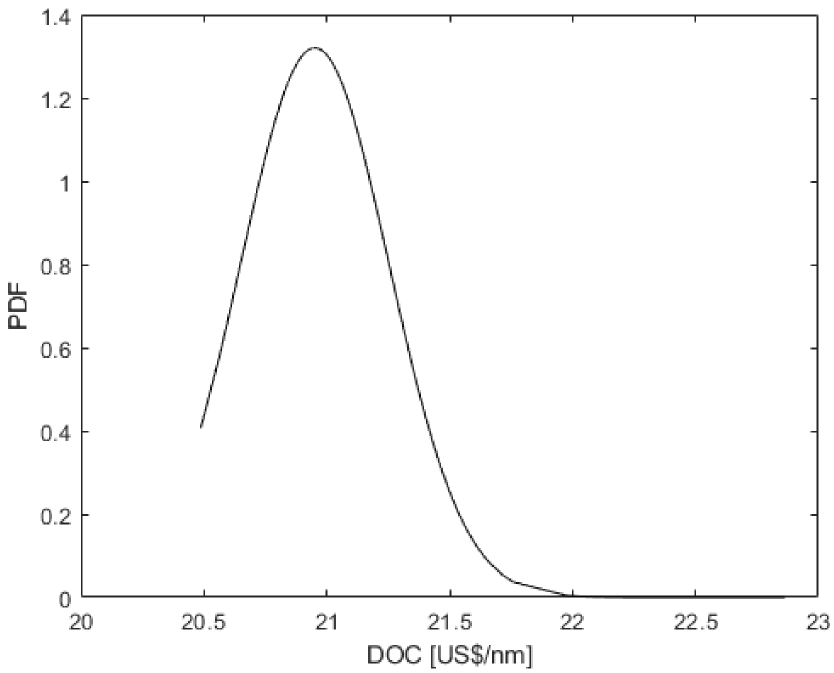

Figure 34: Probability density function of the average DOC

5. Conclusions

An unsupervised learning classification computational tool based on entropy statistics was implemented. It was applied to jet airliners that saw service since the 1950s and proved to be reasonable in most cases. Although correct according to the fundamentals of diffusion and convergence coefficients, the resulting classification of the Boeing 777-300ER airliner indicates that the classification provided by that tool must be confronted with other methodologies of different nature to provide an ultimate label for a product.

The entropy statistics variables that were employed here for a product definition are a considerable improvement from those utilized by Frenken in his inspirational work. The variables of the present work are related to propulsion, airplane size and capacity, airplane performance, and some configuration topology. Certainly, additional variables are needed to map the technological evolution of airplanes, variables linked to navigation, structures, and hydraulics systems, among many others. Another important observation refers to the importance to represent all airplanes that entered service in the database. The omission of a single airplane or its versions may lead to incorrect labeling of other aircraft, noticeably those that saw service short before and after it.

Optimization tasks were successfully carried out to find out high-efficiency airliners presenting lower DOC than the ones related to existing airplanes, some of them being best sellers but whose basic designs are dated back decades ago. The task was focused on the middle of the market segment. An unsupervised learning algorithm based on entropy statistics was utilized for product classification, comprising four categories, classic, niche, failure, and breakthrough designs.

A classic and a niche design were selected for an MMA, with 192 and 273 passengers accommodated into two classes, respectively.

The classic optimal airplane selected is closer to Boeing 757-200 fitted with RB211-535E4B engines and the passenger cabin layout with a single aisle and 6 seating rows. Its engine by-pass ratio of 6:1 is considerably higher than the one for the B757. For the same mission of the out-of-production MMA airliner, the classic design has an MTOW of approximately 17,500 kg lower than B757-200. The present work does not consider advanced technology such as geared turbofan engines, laminar flow, advanced wing airfoils, and others. Thus, the potential for further improvement is huge.

The niche aircraft features 7 seating rows and three engines. It is closer to a B767-300 configuration in terms of capacity and performance. An analysis of the advantages of a three-engine transport airplane was carried out in the present work.

Future work will consider tail-surface sizing by utilizing stability and controllability criteria, turbofan engines with water injection for lower fuel consumption and NOx emission, and fuselage sizing incorporation ditching regulations. Considering that the DOC will be demanding even more computational effort, Bayesian optimization becomes a more efficient way to handle the optimization problems that were carried out in the present work with genetic algorithms.

References

[1] World Bank, "Air Transport, passenger carried," World Bank, October 2019. [Online]. Available: https://data.worldbank.org/indicator/IS.AIR.PSGR?end=2018&start=2004&year=2016. [Accessed October 2019].

[2] G. Rich, "Boeing's 787 Has Realigned Air Travel; These 5 Routes Show How," Investor's Business Daily, 2018. [Online]. Available: https://www.investors.com/news/boeing-787-new-routes-air-travel-realignment-airbus/. [Accessed April 2021].

[3] International Air Transport Association (IATA), "Aviation Technology Roadmap," IATA, Montreal, Canada, 2013.

[4] Aviation Week, "Boeing's New Midsize Airplane: Low Development Cost, Price Are Key," March 2018. [Online]. Available: https://aviationweek.com/air-transport/boeings-new-midsize-airplane-low-development-cost-price-are-key. [Accessed 09 03 2021].

[5] Great Circle Mapper, "Great Circle Distances Calculator," [Online]. Available: http://www.gcmap.com/. [Accessed 09 03 2021].

[6] E. Torenbeek, Advanced Aircraft Design, Wiley & Sons, 2013.

[7] L. K. Loftin, Subsonic aircraft: Evolution and the matching of size to performance (NASA reference publication), National Technical Information Service, 1980, p. 441.

[8] Y. Sun and H. Smith, "Supersonic Business Jet Conceptual Design in a Multidisciplinary Design Analysis Optimization Environment," in *2018 AIAA/ASCE/AHS/ASC Structures, Structural Dynamics, and Materials Conference*, Kissimmee, Florida, 2018.

[9] K. Frenken and L. Leydesdorff, "Scaling Trajectories in Civil Aviation (1913-1997)," *Research Policy,* vol. 29, pp. 331-348, 1999.

[10] B. S. Mattos, J. A. Fregnani and P. C. Magalhães, Conceptual Design of Green Transport Airplanes, Sharjah, UAE: Bentham Books, 2018.

[11] K. Frenken, "Understanding product innovation using Complex Systems Theory," University of Amsterdam, Amsterdam, 2001.

[12] Mathworks, Inc., "gamultiobj," Mathworks, Inc, 2018. [Online]. Available: https://www.mathworks.com/help/gads/gamultiobj.html. [Accessed August 2019].

[13] Wikipedia, The Free Encyclopedia, "Entropy (statistical thermodynamics)," Wikipedia, The Free Encyclopedia, September 2022. [Online]. Available: https://en.wikipedia.org/wiki/Entropy_(statistical_thermodynamics). [Accessed September 2022].

[14] S. Kullback and R. A. Leibler, "On Information and Sufficiency," *Annals of Mathematical Statistics,* vol. 22, pp. 79-86, 1951.

[15] T. M. Cover and J. A. Thomas, Elements of Information Theory, New York: Wiley&Sons, 1991.

[16] Wikipedia, The Free Wikipedia, "Bregman divergence," Wikipedia, The Free Wikipedia, 2019. [Online]. Available: https://en.wikipedia.org/wiki/Bregman_divergence. [Accessed April 2019].

[17] B. S. Mattos, J. A. Fregnani and J. T. Tomita, "Effects of the 1978 Airline deregulation Act on Aircraft Industry Measured by Entropy Statistics," *Transportes,* pp. 1-19, 2022.

[18] Airfleets.Net, "Aircraft Production List," Airfleets.Net, 2019. [Online]. Available: https://www.airfleets.net/home/. [Accessed 21 08 2019].

[19] Bombardier Aerospace, "Canadair CRJ 100/200 Airport Planning Manual," Bombardier Aerospace, Montreal, 2016.

[20] Airfleets.net, "Production List: Canadair Regional Jet," Airfleets.net, 2017.

[21] Wikipedia, The Free Encyclopedia, "Boeing 777," Wikipedia, The Free Encyclopedia, 2022. [Online]. Available: https://en.wikipedia.org/wiki/Boeing_777. [Accessed September 2022].

[22] Boeing Commercial, "777-200/300 Airplane Characteristics for Airport Planning," Boeing Co., Seattle, 1998.

[23] Airbus SE, "Airbus A340-500/-600 Airplane Characteristics," January 2010. [Online]. Available: https://www.airbus.com/sites/g/files/jlcbta136/files/2021-11/Airbus-Commercial-Aircraft-AC-A340-500_600.pdf. [Accessed August 2022].

[24] M. Grotchmann and K. Grimm, "Classification trees for partition testing," *Journal of Software: Testing, Verification and Reliability,* pp. 63-82, June 1993.

[25] Mathworks, Inc., "fitctree - Fit binary decision tree for multiclass classification," Mathworks, Inc., September 2022. [Online]. Available: https://www.mathworks.com/help/stats/fitctree.html. [Accessed 2022].

[26] J. Chen, A. M. MacEachren and D. J. Peuquet, "Constructing Overview + Detail Dendrogram-Matrix Views," *IEEE Transactions on Visualization and Computer Graphics,* pp. 889-896, 2009.

[27] Boeing Commercial Airplanes, "Boeing 757 Airplane Characteristics for Airport Planning," Boeing, Seattle, 2002.

[28] J. A. Fregnani, B. Mattos and J. A. Hernandes, "Multidisciplinary and Multi-Objective Optimization Considering Aircraft Program Cost and Airline Network," *Journal of Air Transportation,* pp. 21-41, January 2021.

[29] N. Secco and B. Mattos, "Artificial neural networks to predict aerodynamic coefficients of transport airplanes," *Aircraft Engineering and Aerospace Technology,* pp. 211-230, March 2017.

[30] M. Widhalm, A. Ronzheimer and M. Hepperle, "Comparison between Gradient-free and Adjoint Based Aerodynamic Optimization of a Flying Wing Transport Aircraft in the Preliminary Design," in *25th AIAA Applied Aerodynamics Conference*, Miami, 2012.

[31] Z. Saad, "Genetic Algorithm Optimization on an Airfoil using PARSEC Method to Describe the Shape of the Airfoil," Oct 2018. [Online]. Available: https://www.mathworks.com/matlabcentral/fileexchange/69095-optimization-of-an-airfoil-shape-using-genetic-algorithm-ga?s_tid=srchtitle. [Accessed June 2021].

[32] J. Fregnani, B. S. Mattos and J. A. Hernandes, "An Innovative Approach for integrated Airline Network and Aircraft Family Optimization," in *AIAA Aviation Forum 2019*, Dallas, DOI: https://doi.org/10.2514/6.2019-2865, 2019.

[33] I. Chakraborty, T. Nam, J. Gross, D. Mavris, J. Schetz and R. Kapania, "Comparative Assessment of Strut-Braced and Truss-Braced Wing Configurations Using Multidisciplinary Design Optimization," *Journal of Aircraft,* pp. 2009-2020, 2015.

[34] R. Priem, H. Gagnon, I. Chittick, S. Dufresne, Y. Diouane and N. Bartoli, "An Efficient Application of Bayesian Optimization to an Industrial MDO framework for Aircraft Design," in *AIAA AVIATION 2020 FORUM*, Virtual Event, 2020.

[35] R. Garnett, Bayesian Optimization, Cambridge: Cambridge University Press, 2022.

[36] İ. Yanıkoğlu, B. Gorissen and D. den Hertog, "A survey of adjustable robust optimization," *European Journal of Operational Research,* pp. 799-813, September 2019.

[37] J. Garcia and A. Peña, "Robust Optimization: Concepts and Applications," in *Nature-inspired Methods for Stochastic, Robust and Dynamic Optimization*, United Kingdom, InterchOpen, 2018.

[38] D. Bertsimas and M. Sim, "The Price of Robustness," *Operations Research,* pp. 35-53, 2004.

[39] A. Rios, J. Fregnani, B. Mattos and M. Condé, "Identification of the Actual Mission Profiles and Their Impact on the Integrated Aircraft and Airline Network Optimization," 2021.

[40] V. Loureiro and B. S. Mattos, "Powerplant as Design Variable for Multi-disciplinary Design Optimization of Transport Airplane," in *27th AIA Applied Aerodynamics Conference*, San Antonio, 2009.

[41] J. Fregnani, B. Mattos and J. Hernandes, "Multidisciplinary and Multi-Objective Optimization Considering Aircraft Program Cost and Airline Network," *Journal of Air Transportation,* pp. 27-41, January 2021.

[42] R. Langton, C. Clark, M. Hewitt and L. Richards, Aircraft Fuel Systems, John Wiley & Sons, 2009.

[43] B. Singh, "A Medium-Fidelity Method for Rapid Maximum Lift Estimation," Delft University, Delft, 2017.

[44] M. Drela, "XFOIL - Subsonic Airfoil Development System," October 2018. [Online]. Available: http://web.mit.edu/drela/Public/web/xfoil/. [Accessed October 2018].

[45] S. Gudmundsson, "Maximum Lift Coefficient," Elsevier, 2018. [Online]. Available: https://www.sciencedirect.com/topics/engineering/maximum-lift-coefficient. [Accessed September 1029].

[46] R. C. Quintero, "TECHNO-ECONOMIC AND ENVIRONMENTAL Techno-Economic and Environment Risk Assessment of Innovative Propulsion Systems for Short-Range Civil Aircraft," Cranfield, 2009.

[47] MathWorks, "Genetic Algorithm," MathWorks, December 2017. [Online]. Available: https://www.mathworks.com/discovery/genetic-algorithm.html. [Accessed December 2017].

[48] Jane's, "Jane's Aero Engines," IHS Markit, December 2017. [Online]. Available: https://janes.ihs.com/.

[49] Wikipedia, The Free Encyclopedia, "Airbus A320 family," Wikipedia, The Free Encyclopedia, 2021. [Online]. Available: https://en.wikipedia.org/wiki/Airbus_A320_family. [Accessed March 2021].

[50] Airbus SE, "Airbus A320 Aircraft Characteristics and Maintenance Planning," Airbus, Blagnac, 2017.

[51] Modern Airliners, "Airbus A320 Specs – What is behind one of the most popular short-haul airliners?," Modern Airliners, March 2021. [Online]. Available: https://modernairliners.com/airbus-a320-introduction/airbus-a320-specs/. [Accessed 2021].

[52] Wikipedia, The Free Encyclopedia, "Rolls-Royce RB211," Wikipedia, The Free Encyclopedia, 2021. [Online]. Available: https://en.wikipedia.org/wiki/Rolls-Royce_RB211. [Accessed May 2021].

[53] European Union Aviation Safety Agency, "Type-Certificate Data Sheet for Rolls&Royce for RB211-535 Series Engine," EASA, Cologne, 2020.

[54] Boeing Commercial Airplanes, "Boeing Resources," 2021. [Online]. Available: https://www.boeing.com/resources/boeingdotcom/company/about_bca/startup/pdf/historical/757_passenger.pdf. [Accessed May 2021].

[55] Z. Saad, "Genetic Algorithm Optimization on an Airfoil using PARSEC Method to Describe the Shape of the Airfoils," Oct 2018. [Online]. Available: https://www.mathworks.com/matlabcentral/fileexchange/69095-optimization-of-an-airfoil-shape-using-genetic-algorithm-ga?s_tid=srchtitle. [Accessed June 2021].

[56] Boeing Commercial, "747-400 Airplane Characteristics for Airport Planning," Boeing Co., Seattle, 2002.

[57] Wikipedia, The Free Encyclopedia, "McDonnell Douglas DC-10," Wikipedia, The Free Encyclopedia, March 2021. [Online]. Available: https://en.wikipedia.org/wiki/McDonnell_Douglas_DC-10. [Accessed March 2021].

[58] Boeing Commercial Airplanes, "757-200/300 Airplane Characteristics for Airport Planning," Boeing Co., Seattle, 2002.

[59] Boeing Commercial Airplanes, "767 Airplane Characteristics for Airport Planning," Boeing Co., Seattle, 2005.

[60] "Falcon 900LX," Dassault Aviation, 2021. [Online]. Available: https://www.dassaultfalcon.com/en/Aircraft/Models/900LX/Pages/overview.aspx. [Accessed March 2021].

[61] Gulfstream Aerospace, "Gulfstream G550," Gulfstream Aerospace, 2021. [Online]. Available: https://www.gulfstream.com/en/aircraft/gulfstream-g550/. [Accessed March 2021].

[62] Dassault Aviation, "Falcon 6X," Dassault Aviation, 2021. [Online]. Available: https://www.dassaultfalcon.com/en/Aircraft/Models/6X/Pages/overview.aspx. [Accessed March 2021].

[63] Embraer Executive Jets, "Embraer Legacy 650," 2021. [Online]. Available: https://www.basjets.com/de/Flugzeugkauf/Neuflugzeuge/Long-Range-Jets/Embraer-Legacy-650. [Accessed March 2021].

[64] G. W. van Bondergraven, "Commercial Aircraft DOC Methods," in *AIAA/AHS/ASEE Aircraft Design Systems and Operations Conference*, Dayton, 1990.

[65] Air Transport Association of America, "Standard Method of Estimating Comparative Operating Direct Costs of Turbine Powered Transport Airplanes," Air Transport Association of America, Washington, D. C., 1967.

[66] "Jet Fuel Price Monitor," IATA, May 2021. [Online]. Available: https://www.iata.org/en/publications/economics/fuel-monitor/. [Accessed May 2021].

[67] D. Howe, Aircraft Conceptual Design Synthesis, London and Bury St Edmunds: Professional Engineering Publishing Limited, 2000.

[68] M. Gumes e L. D. Andrade Pereira, “Utilização de Redes Neurais para Estimação de Coeficienets Aerodinâmicos e Derivadas de Estabilidade,” Undegraduation thesis, Instituto tecnológico de Aeronáutica,, São José dos Campos, 2019.

[69] B. S. Mattos, F. A. Bortolete, J. A. T. Fregnani, A. B. Jorge, W. M. Alves and R. V. Cruz, "Application of Machine Learning and Multi-Disciplinary/Multi-Objective Optimization Techniques for Conceptual Aircraft Design," in *Model-Based and Signal-Based Inverse, Vol. I*, Brasília, D.F., University of Brasilia, 2022, pp. 143-236.